Stem Cell Reports
Resource
ISSCR
OPEN ACCESS

Homozygous might be hemizygous: CRISPR/Cas9 editing in iPSCs results in detrimental on-target defects that escape standard quality controls

Dina Simkin,[1] Vasileios Papakis,[1] Bernabe I. Bustos,[1,2] Christina M. Ambrosi,[3] Steven J. Ryan,[3] Valeriya Baru,[3] Luis A. Williams,[3] Graham T. Dempsey,[3] Owen B. McManus,[3] John E. Landers,[4] Steven J. Lubbe,[1,2] Alfred L. George, Jr.,[5] and Evangelos Kiskinis[1,6,7,*]

[1]The Ken & Ruth Davee Department of Neurology, Feinberg School of Medicine, Northwestern University, Chicago, IL 60611, USA
[2]Simpson Querrey Center of Neurogenetics, Feinberg School of Medicine, Northwestern University, Chicago, IL 60611, USA
[3]Q-State Biosciences, Cambridge, MA 02139, USA
[4]Department of Neurology, University of Massachusetts Medical School, Worcester, MA 01605, USA
[5]Department of Pharmacology, Feinberg School of Medicine, Northwestern University, Chicago, IL 60611, USA
[6]Simpson Querrey Institute, Northwestern University, Chicago, IL 60611, USA
[7]Department of Neuroscience, Feinberg School of Medicine, Northwestern University, Chicago, IL 60611, USA
*Correspondence: evangelos.kiskinis@northwestern.edu
https://doi.org/10.1016/j.stemcr.2022.02.008

SUMMARY

The ability to precisely edit the genome of human induced pluripotent stem cell (iPSC) lines using CRISPR/Cas9 has enabled the development of cellular models that can address genotype to phenotype relationships. While genome editing is becoming an essential tool in iPSC-based disease modeling studies, there is no established quality control workflow for edited cells. Moreover, large on-target deletions and insertions that occur through DNA repair mechanisms have recently been uncovered in CRISPR/Cas9-edited loci. Yet the frequency of these events in human iPSCs remains unclear, as they can be difficult to detect. We examined 27 iPSC clones generated after targeting 9 loci and found that 33% had acquired large, on-target genomic defects, including insertions and loss of heterozygosity. Critically, all defects had escaped standard PCR and Sanger sequencing analysis. We describe a cost-efficient quality control strategy that successfully identified all edited clones with detrimental on-target events and could facilitate the integrity of iPSC-based studies.

INTRODUCTION

The ability to correct disease-associated genetic variants in patient-specific induced pluripotent stem cells (iPSCs) or to insert pathogenic variants into healthy control iPSCs by CRISPR/Cas9 has enabled the development of cellular models that can be used to interrogate the relationship between genotype and phenotype in differentiated, disease-relevant cells. Correcting a disease-associated mutation in a patient iPSC line can demonstrate a causal relationship between the mutation and a cellular phenotype, while introducing a mutation in a healthy control iPSC line can assess its sufficiency for a particular phenotype. The generation of isogenic pairs of iPSC lines is quickly becoming an essential prerequisite in disease modeling studies, as the genetic background of reprogrammed iPSC lines may confound phenotypic analysis of differentiated disease-relevant cells (Ichida and Kiskinis, 2015; Merkle and Eggan, 2013). However, editing genes without undesired genomic effects in iPSCs remains difficult (Kwart et al., 2017) and requires significant resources and expertise that often challenge research laboratories that are focused on using these cells as a tool to study human development or disease mechanisms.

Precise genome editing is achieved by inducing CRISPR/Cas9-mediated double-stranded DNA breaks (DSBs) targeted to a specific location by a single-guide RNA (sgRNA; Sander and Joung, 2014). While the exact repair mechanisms in human cells remain poorly defined, DSBs are likely repaired by non-homologous end joining (NHEJ) or homology-directed repair (HDR). HDR can occur through the supply of an exogenous donor sequence as a template or through homologous recombination with an endogenous allele on the sister chromatid (which can lead to copy-neutral loss of heterozygosity [LOH]; Bibikova et al., 2003; Liang et al., 1998; Mao et al., 2008; Shrivastav et al., 2008). The efficiency of successful HDR in human iPSCs is highly variable (e.g., 2%–20%), and more than 80% of selected clones following genotype screening contain unwanted genomic defects, such as insertions, deletions, inversions, and rearrangements (Byrne et al., 2014; Maguire et al., 2019; Martin et al., 2019; Santos et al., 2016). Many approaches have been employed to improve the odds of achieving the intended edit and reduce the burden of screening hundreds of clones (Blair et al., 2016; Hockemeyer and Jaenisch, 2016; Ikeda et al., 2018; Kwart et al., 2017; Merkle et al., 2015; Popp et al., 2018; Steyer et al., 2018). These include strategic design of sgRNAs and single-stranded oligo donors (ssODNs), and the use of positive selection markers for flow cytometry sorting or antibiotic selection (for extended reviews, see Mianne et al., 2020; Wang et al., 2018). Nevertheless, most protocols still require large-scale screening of 25–100 isolated clones (Paquet et al., 2016). This labor-intensive step is typically done

by PCR amplification of a few hundred bases spanning the target locus, followed by Sanger sequencing.

A major concern has been the potential off-target edits that CRISPR/Cas9 might introduce because of sequence homology of the sgRNA to other regions in the genome (Cho et al., 2014; Fu et al., 2013; Hsu et al., 2013; Pattanayak et al., 2013). Recent studies have highlighted the incidence of large deletions, insertions, and intricate genomic rearrangements at or within a short distance from the targeted site (Adikusuma et al., 2018; Kosicki et al., 2018; Leibowitz et al., 2021; O'Keefe et al., 2010; Owens et al., 2019; Shin et al., 2017). These deleterious on-target events, which likely occur through NHEJ, microhomology-mediated end joining (MMEJ), and homologous recombination (Fu et al., 2021; Wang and Xu, 2017), have been extensively described in mice (Kosicki et al., 2018) and human embryos (Alanis-Lobato et al., 2021; Liang et al., 2020; Ma et al., 2017; Zuccaro et al., 2020) and have also been shown to occur in human iPSCs (Blondal et al., 2021; Weisheit et al., 2020). The frequency and nature of on-target defects in CRISPR/Cas9-edited iPSC lines have not been widely interrogated by multiple groups. In the most comprehensive study to date, Weisheit et al. (2020) examined 35 iPSC clones edited across 3 genomic locations and identified on-target defects in 18%–40% of cases. Additionally, CRISPR/Cas9 can cause chromosomal instability, which can result in copy loss or copy-neutral LOH (Alateeq et al., 2018; Gorter de Vries et al., 2019; Hajiahmadi et al., 2019; Korablev et al., 2020; Ledford, 2020; Prat et al., 2020; Przewrocka et al., 2020; Rayner et al., 2019; Weisheit et al., 2020; Yang et al., 2017; Zischewski et al., 2017). Importantly, genotyping using PCR and Sanger sequencing of a short DNA fragment serves well as an initial screen, but may lead to false identification of edited clones, as large on-target insertions/deletions may cause exclusive amplification of only one allele. Such allelic dropout events constitute a known limitation of PCR-based approaches (Shestak et al., 2021).

Here, we evaluated 27 iPSC clones generated from 9 different CRISPR/Cas9 targeting events across 4 disease-associated genes (*KCNQ2*, *SCN1A*, *NEK1*, and *DNAJC7*). Critically, all these clones were deemed to be "correctly" edited during initial screening, as judged by PCR amplification of short ~200 bp fragments and Sanger sequencing of the targeted region. We found that 33% had acquired complex, on-target genomic alterations, including large insertions and copy-neutral LOH. A combination of simple-to-execute assays including allele copy number quantitative genotyping PCR (qgPCR) and assessment of heterozygosity through sequencing of nearby heterozygous single nucleotide polymorphisms (SNPs) successfully identified all lines that had appeared to be correctly edited, but were, in fact, defective. Our findings are in accordance with recent reports (Weisheit et al., 2020, 2021) and further highlight the need for standardized quality control (QC) of CRISPR/Cas9-edited iPSC lines (for an overview of QC practices for iPSCs, see Steeg et al., 2021).

RESULTS

CRISPR/Cas9 editing can cause detrimental on-target insertions in iPSCs: a case study of apparently correctly edited clones

We reprogrammed peripheral blood mononuclear cells (PBMCs) isolated from a pediatric epilepsy patient with a heterozygous mutation (c.821C > T; p.T274M) in the *KCNQ2* gene to generate a patient-specific iPSC line. We produced several isogenic mutation-corrected control lines by CRISPR/Cas9 editing. In parallel to correcting the disease-causing mutation, we introduced a silent Cas9-blocking mutation at the cut site to reduce CRISPR/Cas9 re-cutting (Figure 1A and Table S1; Paquet et al., 2016). CRISPR/Cas9-blocking mutations have been shown to increase the efficiency of on-target editing up to 10-fold (Okamoto et al., 2019; Paquet et al., 2016). To avoid any unintended effects of the silent mutation on protein expression, we consulted the human codon usage frequency table to select a codon of similar usage frequency (Dhindsa et al., 2020). To screen for clones with the desired edit, we used PCR amplification and Sanger sequencing of 264 bp around the targeted region (Table S2). The initial screening of more than 50 single isolated edited clones revealed several that appeared to be homozygous for the wild-type (WT) *KCNQ2* allele sequence, one of which carried the designed Cas9-blocking mutation (Figures 1B and 1C). This type of initial screening is common practice and allows for discarding clones with short deleterious edits, including insertions/deletions or mutations less than 200 bp in length. We selected 2 "corrected" clones for further characterization (*KCNQ2-01-G6* and *KCNQ2-01-A6*). To identify any short duplications or inversions and to further validate the correction of the patient mutation, we amplified a larger PCR fragment (~1.2 Kb) encompassing the targeted region and performed Sanger sequencing (Figure S1). Analysis of the larger PCR fragment confirmed the apparent correction of the disease-causing variant (Figure S1). Both corrected clones exhibited a normal karyotype as determined by standard G banding and digital KaryoStat analysis (Figure S2) and had DNA short tandem repeat (STR) profiles that matched the parental untargeted patient lines as determined by DNA fingerprinting (Figure S3). Moreover, evaluation by PCR and either T7E1 or Sanger sequencing analysis of the top 11 genomic regions with homology to the sgRNA used for targeting the *KCNQ2* locus did not reveal any evidence of off-target edits (Figure S4 and Table S3).

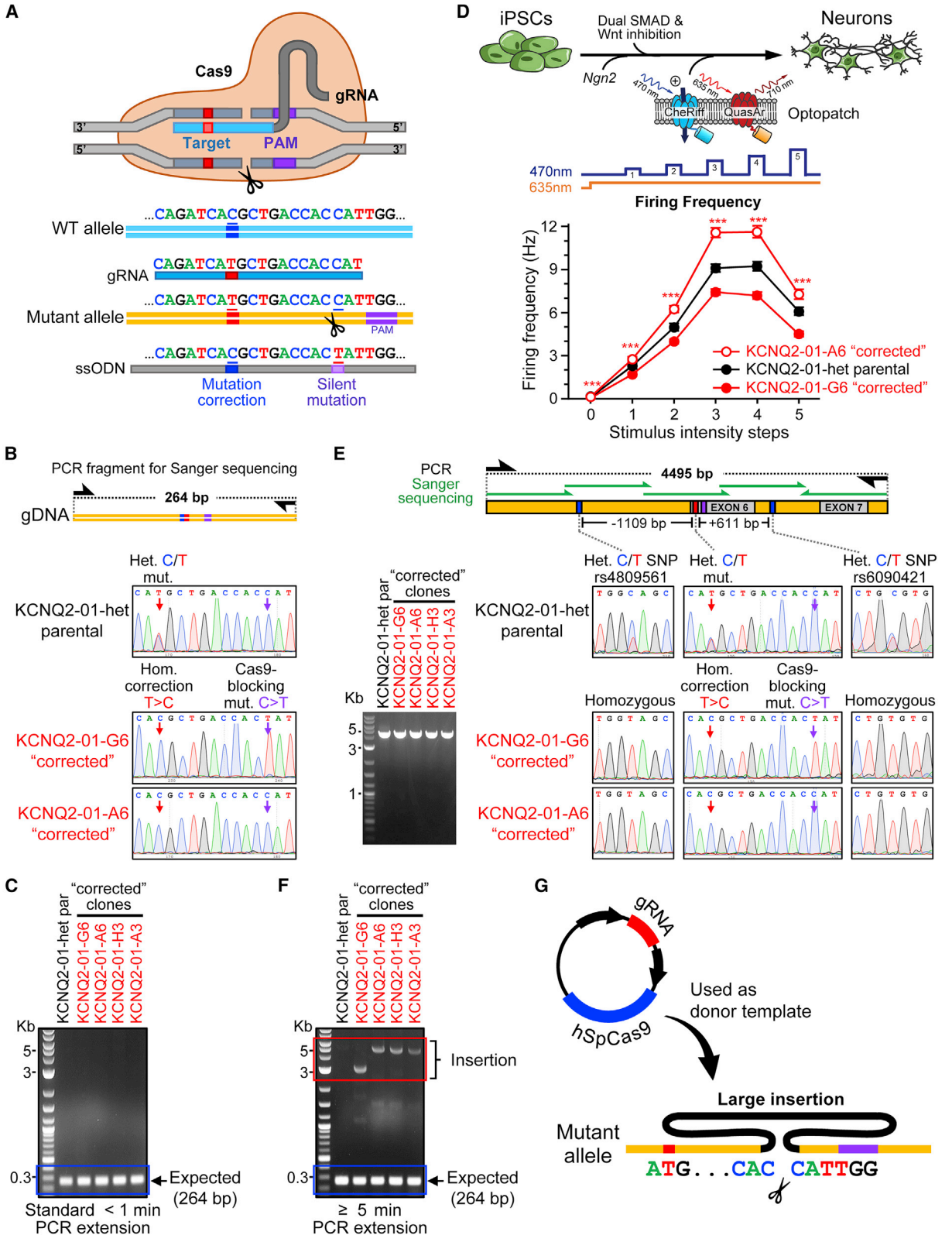

(legend on next page)

We next proceeded to perform functional phenotyping assays on cortical excitatory neurons differentiated from the two corrected iPSC clones (*KCNQ2-01-G6* and *KCNQ2-01-A6*) and the parental patient line (*KCNQ2-01-het-par*). To examine the firing frequency of large numbers of neurons, we used the Optopatch platform, a system for high-throughput, all-optical electrophysiology with single cell resolution (Hochbaum et al., 2014; Kiskinis et al., 2018; Werley et al., 2017). The combined expression of CheRiff (a blue-light-activated channelrhodopsin) and QuasAr3 (a fluorescent voltage indicator) allows for the simultaneous stimulation and recording from multiple neurons within an elaborate network (Figure 1D). Using *Synapsin* promoter-driven expression constructs for CheRiff and QuasAr3, we imaged and analyzed the firing frequency of more than 10,000 neurons per cell line under a blue-light illumination protocol (Figures 1D and S5). After 35 days in culture, neurons were monitored for 2 s without stimulation followed by five 500-ms pulses of blue light of increasing intensity (Figure 1D, middle). As shown by the average firing rates of neurons (Figures 1D and S5), *KCNQ2-01-G6* and *KCNQ2-01-A6* exhibited opposing behavior in reference to parental patient-derived neurons. *KCNQ2-01-G6* exhibited a significantly lower firing frequency, whereas *KCNQ2-01-A6* neurons exhibited higher firing frequency relative to parental-derived neurons across the protocol (Figures 1D and S5).

This divergent electrophysiological behavior prompted us to investigate its origin. Close inspection of Sanger sequencing data of long-range PCR fragments (~4.5 Kb) around the edited locus revealed that the corrected clones were homozygous for SNPs and short intronic indels flanking the edited locus, which were heterozygous in the parental untargeted cell line (Figure 1E). This apparent LOH suggested the occurrence of either copy-neutral LOH through homologous recombination with an endogenous allele or allelic dropout resulting from introduction of a monoallelic structural variant such as a large insertion or deletion that would compromise primer binding or PCR amplification. Indeed, PCR amplification of the targeted region using longer extension times revealed the presence of large monoallelic insertions ranging from 3 to 5 Kb within the 2 corrected clones as well as within 2 additional clones from the same targeting experiment (Figure 1F). Gel extraction, purification, and Sanger sequencing of the inserted DNA revealed inserted segments corresponding to the plasmid used to express Cas9 (Figures 1G and S6). Each of the 4 edited clones (*KCNQ2-01-G6*, *-A6*, *-A3*, and *-H3*) had incorporated different segments of Cas9 plasmid DNA at the targeted locus. Thus, standard PCR and Sanger sequencing protocols were misleading because they failed to distinguish between a true homozygously edited clone and one where a monoallelic structural variant caused allelic dropout (Figure S7). Critically, our inability to initially detect the deleterious structural variants within the *KCNQ2* gene confounded our subsequent electrophysiological phenotyping experiments.

Figure 1. Standard QC methods fail to detect HDR-mediated large on-target defects in human iPSCs

(A) Illustration of Cas9 with sgRNA and ssODN and editing strategy for correction of *KCNQ2* heterozygous mutation in patient-specific iPSCs (*KCNQ2-01-het parental*).

(B) Genotype screening of single CRISPR/Cas9 targeted iPSC clones was done by PCR amplification of 264 bp spanning the targeted site. Bottom: Sanger sequencing of gDNA PCR amplicons show *KCNQ2-01-het* parental iPSC line with a heterozygous mutation and mutation "correction" in 2 edited clones (*KCNQ2-01-G6* and *KCNQ2-01-A6*). The absence of larger indels around the target site was validated by PCR amplification and Sanger sequencing of a larger fragment.

(C) A 264 bp fragment flanking the *KCNQ2-01* target locus was PCR amplified using standard PCR extension times. A single band of expected size is visible when PCRs were run on an agarose gel.

(D) *KCNQ2-01-het-par* and corrected clones *-G6* and *-A6* iPSCs were differentiated into cortical excitatory neurons and transduced with CheRiff and QuasAr3 for all-optical electrophysiology (Optopatch) experiments. The well-wide average firing frequency of neurons (~85 neurons per well, ~4,000 neurons total) upon blue light stimulation with increasing intensity steps was analyzed across one independent experiment and two others (see Figure S5). *KCNQ2-01-G6* and *-A6* neurons exhibited significantly lower and higher firing frequencies, respectively, relative to *KCNQ2-01-het* parental patient-derived neurons across the stimulation protocol and independent experiments. *Indicates significant difference between *KCNQ2-01-A6 and KCNQ2-01-G6* neurons (*$p < 0.05$, **$p < 0.005$, and ***$p < 0.0005$). All data are reported as mean ± SEM ($n = 48$ wells analyzed per cell line, $N = 1$ experiment; 2 additional independent experiments are presented in Figure S5).

(E) Left: Agarose gel electrophoresis of 4,495 bp PCR amplified fragment reveals a single band from *KCNQ2-01-het* parental iPSC line and isogenic corrected clones. Right: Sanger sequencing in ~850 bp steps across the 4.5 Kb PCR fragment revealed heterozygous SNPs in the *KCNQ2-01-het* parental unedited iPSC line on both sides of the target locus that were not present in corrected clones.

(F) A 264 bp fragment flanking the *KCNQ2-01* target locus was PCR amplified using long duration PCR extension times. Agarose gel electrophoresis revealed the presence of large (3–5 Kb) insertions in all edited clones that had appeared to be corrected using standard PCR/Sanger sequencing in (B) and (C) (see Figures S6–S8).

(G) Non-homologous or microhomology-mediated end joining can result in large insertions by using exogenously supplied Cas9 plasmid DNA as the donor template (see also Figures S1–S8).

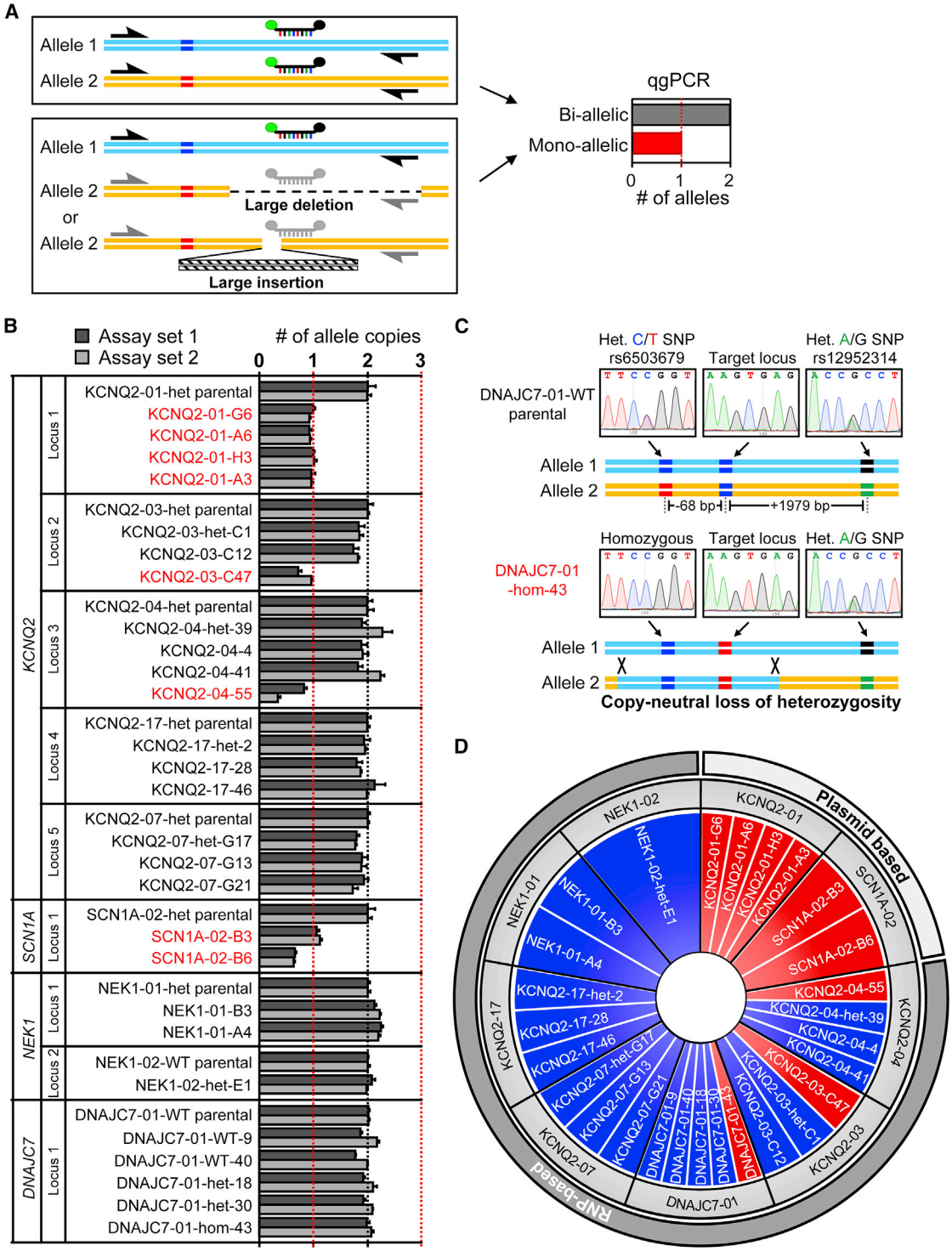

Figure 2. Assessment of genomic allele copy number

(A) Illustration of qgPCR assay. Large deletions prevent primer or probe binding, and large insertions prevent PCR extension and thus reveal amplification of only one allele.

(B) qgPCR assay was used to assess allele copy numbers in 27 CRISPR/Cas9 edited clones. Eight out of 27 (30%) clones were found to be monoallelic. Data are represented as mean ± SEM (n = 3 technical replicates).

(legend continued on next page)

Large on-target genomic defects are a common feature of CRISPR/Cas9-edited iPSC lines

Our discovery of falsely corrected clones for *KCNQ2-01* prompted us to investigate a larger set of CRISPR/Cas9-edited iPSC lines that we had generated. We examined 27 iPSC clones produced after CRISPR/Cas9 editing of 9 separate genomic regions within 4 genes (*KCNQ2*, *SCN1A*, *DNAJC7*, and *NEK1*). For 7 out of 9 regions, CRISPR/Cas9 was used to correct a disease-associated mutation, while in the remainder, CRISPR/Cas9 was used to introduce a disease-associated mutation. As recently recommended by Weisheit et al. (2020), we used qgPCR assays to evaluate the targeted allele copy number as an initial screening approach (Figure 2A). This assay is more scalable compared with long-range PCR, which in some cases requires troubleshooting with different primer sets to amplify the desired fragment with high specificity. We designed 2 independent sets of primers with probes that amplified 300–400 bp around each respective targeted locus that in most cases were at least 100 bp away from the cut site (Table S4). In the qgPCR assay, large deletions or insertions in the target region prohibit amplification of the affected allele, and thus such clones exhibit higher cycle threshold (Ct) values corresponding to a reduced allele copy number (Figure 2A). After normalization to an internal reference gene (*TERT*), the Ct value detected in each edited clone was compared with the value of its own parental, untargeted cell line. Of the 27 clones that were deemed to be correctly edited by short PCR/Sanger sequencing, we identified 8 that exhibited significantly lower allele copy numbers (Figure 2B). As an additional QC assay, we evaluated all targeted clones that appeared to be biallelic with the qgPCR assay for the presence of heterozygous SNPs within long-range PCR fragments (4–11.5 Kb) spanning the targeted locus. We identified one clone (*DNAJC7-01-hom-43*) that lacked a nearby upstream heterozygous SNP (dbSNP:rs6503679; −68 bp away from the target site), which was present in its respective parental iPSC line (Figure 2C). Critically, we found that a downstream heterozygous SNP (dbSNP:rs12952314; +1979 bp from target) was present in both the parental untargeted iPSC line and the *DNAJC7-01-hom-43* clone. The fact that this line had a normal allele copy number (Figure 2B) yet was homozygous for a parental heterozygous SNP suggests that CRISPR/Cas9 editing caused on-target and upstream copy-neutral LOH.

The qgPCR assays revealed that 33% of targeted clones acquired complex on-target genomic defects that escaped detection by standard PCR/Sanger sequencing (Figure 2D). We next employed a longer PCR extension strategy of short (200–500 bp) amplicons coupled to Sanger sequencing to further examine the defects in the same cohort of iPSC clones (Figure S8). We found that clone *KCNQ2-03-C47* had a large (>10 Kb) insertion of mtDNA, while clone *SCN1A-02-B6* had acquired a complex rearrangement. While long-range PCR and qgPCR assays suggested monoallelic PCR amplification and the potential presence of structural variants in clones *KCNQ2-04-55* and *SCN1A-02-B3,* we were not able to detect any abnormalities through long extension PCR (Figure S8). Our collective QC analyses revealed that most compromised clones appeared to have large on-target insertions, which included parts of the Cas9 plasmid used for targeting (Figures 1G and S6) or portions of mtDNA (Figure S8). Critically, we found that deleterious on-target defects occurred independently of the method used to deliver Cas9, as there were problematic clones edited with a plasmid (*KCNQ2-01* and *SCN1A-02*) as well as ones edited with recombinant proteins (*KCNQ2-03*, *KCNQ2-04*, and *DNAJC7-01*) (Figure 2D).

Whole-genome sequencing identifies deleterious on-target defects

We next investigated whether whole-genome sequencing (WGS) would allow us to identify deleterious on-target effects including large insertions of exogenous (e.g., Cas9 plasmid) and endogenous DNA (e.g., mtDNA or other chromosomal DNA) and copy-neutral LOH. WGS does not rely on targeted PCR-based primer binding for amplification and therefore is not subject to allelic dropout. Instead, DNA libraries are prepared using complete genomic DNA (gDNA) that is fragmented into short segments and ligated to adaptor sequences at each end (Figure 3A). Primers corresponding to the adaptor sequences are used to unbiasedly amplify the gDNA fragments by PCR for library preparation and sequencing from each end of the fragments (typically 150 bp is sequenced from each end in paired-end WGS). However, large insertions such as the ones we found here are difficult to identify using typical short read paired-end WGS because reads that do not align within the reference genome are routinely discarded during the alignment to a

(C) A 4.4 Kb fragment spanning the targeted locus was PCR amplified and subjected to Sanger sequencing to identify the presence of heterozygous SNPs. Sequencing of *DNAJC7-01-WT* parental line revealed presence of upstream and downstream heterozygous SNPs. Sequencing of *DNAJC7-01-hom-43* homozygously edited clone revealed absence of upstream heterozygous SNP indicating a copy neutral LOH (see Figure 6).

(D) Donut chart of edited clones representing 9 targeting events and numbers of clones found to be correctly edited (blue) and clones with unwanted monoallelic editing (red) (see also Figures 6 andS8).

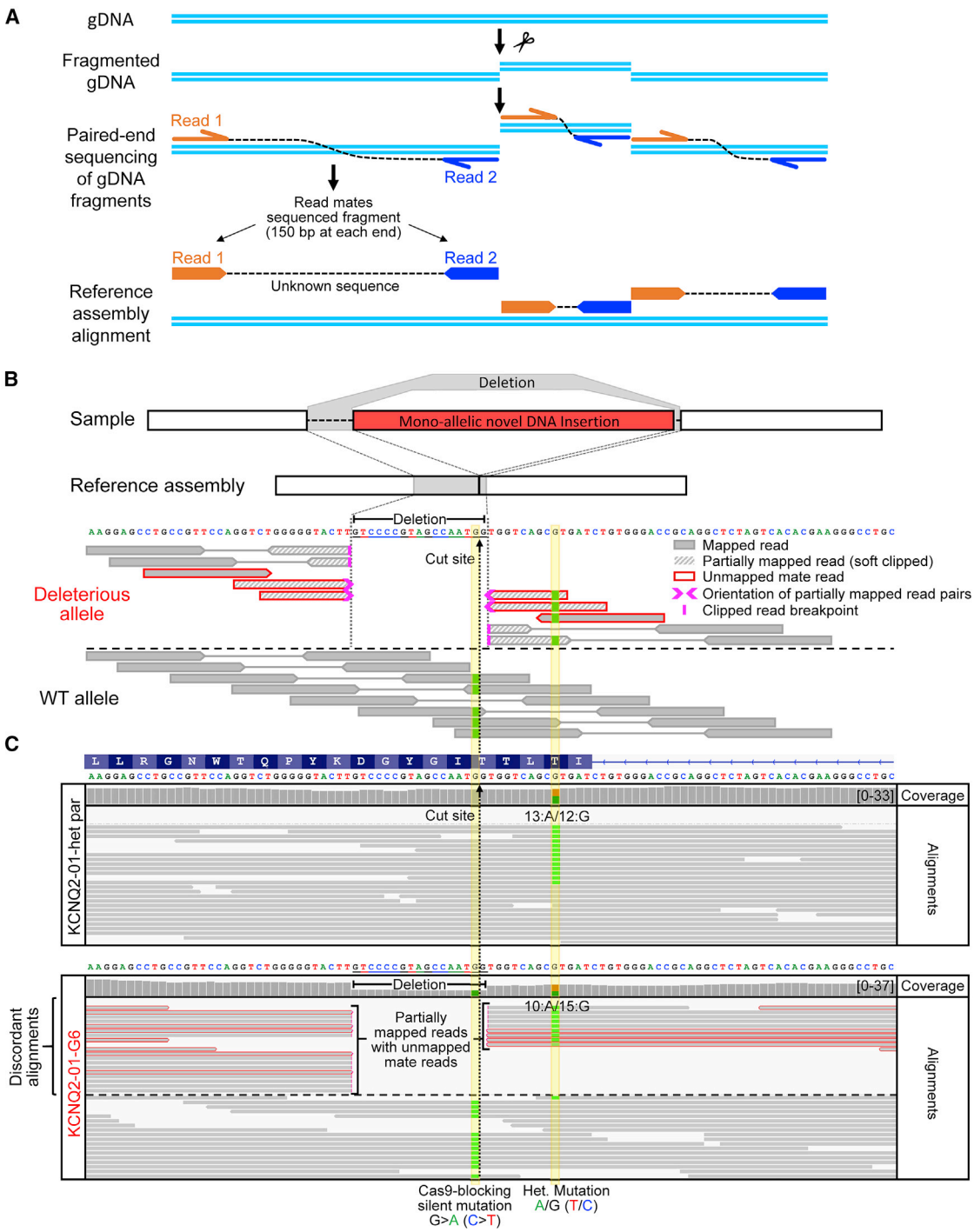

Figure 3. WGS can help identify specific deleterious on-target effects of CRISPR/Cas9 editing and detect clones falsely identified as corrected

(A) Illustration of paired-end WGS. gDNA is fragmented into random size fragments, and then 150 bp are sequenced from both ends; the insert between the sequenced reads is unknown. Read mate sequences are aligned to a reference genome assembly.

(B) Illustration of paired-end WGS alignments in the presence of a monoallelic structural variant such as the large on-target insertion in *KCNQ2-01-G6*. A short 17 bp deletion was also introduced around the cut site.

(C) WGS Integrative Genomic Viewer (IGV) plot showing human genome (T2T) reference assembly mapped sequencing reads around the targeted locus of *KCNQ2-01-het-parental* and *-G6* edited line. WGS analysis revealed the presence of the heterozygous patient mutation in

(legend continued on next page)

reference genome assembly (Van der Auwera et al., 2013; Van der Auwera and O'Connor, 2020).

We sequenced or re-analyzed (Simkin et al., 2021) WGS data from 13 iPSC lines including parental untargeted and edited clones, with or without defects (Table S5). Sequence reads were aligned to the new CHM13 T2T human genome reference assembly (Nurk et al., 2021), in which long read sequencing was used to fill in the gaps of the previous reference assembly. Using Integrated Genome Viewer (IGV) software, we identified deleterious on-target effects of CRISPR/Cas9 editing in all the falsely edited clones examined. By grouping the sequencing alignment reads by "reference concordance," reads that were partially mapped (split reads), or reads with mates that did not map to the reference sequence owing to exogenous DNA insertions (in paired-end sequencing), became easy to spot (Figures 3, 4, 5, and 6, Figure S9). The presence of discordant reads signifies the potential presence of a structural variant.

Careful analysis of the edited locus of line *KCNQ2-01-G6* confirmed that it had a monoallelic novel DNA insertion of Cas9 plasmid DNA at the target site that was flanked by short deletions and that the heterozygous disease-associated mutation was not corrected (Figures 3B and 3C). In stark contrast to the parental line, *KCNQ2-01-G6* showed many discordant alignments. These included a drop in coverage around the deletion and several partially mapped reads with unmapped mate reads (Figures 3B and 3C). WGS of clone *KCNQ2-01-A6* revealed that the patient mutation was also not corrected and that it had similarly acquired a novel monoallelic DNA insertion (Figure S9). This was apparent by the frequency of discordant alignments that included partially mapped reads with unmapped mate reads as well as ones that partially mapped to a region on human chromosome 4. Analysis of clone *KCNQ2-04-55* revealed a monoallelic insertion of mtDNA (Figure 4), while clone *KCNQ2-03-C47* had a short 10 bp deletion adjacent to another monoallelic mtDNA insertion (Figure 5). Lastly, WGS enabled us to verify that CRISPR/Cas9 editing had caused copy-neutral LOH in clone *DNAJC7-01-hom-43* as well as define the boundaries of this loss through inspecting for the presence of heterozygous SNPs (Figure 6).

A cost-efficient strategy for evaluating edited iPSC lines

Given the high incidence of complex on-target genomic defects we detected in edited human iPSC lines, there is a need to design a time- and cost-efficient QC strategy to successfully identify detrimental events and facilitate the integrity of subsequent experiments. Because CRISPR/Cas9 gene editing efficiency is low and there is a need to screen many clones, initial selection is typically based on PCR coupled to Sanger sequencing (Figure 7). During this first selection process, the presence of any heterozygous bases (whether a heterozygous SNP or an introduced silent heterozygous mutation) within the PCR fragment sequence demonstrates biallelic amplification. Thus, when nearby heterozygous SNPs are present near the targeted locus in parental gDNA, the most efficient way to confirm on-target editing and biallelic amplification is to amplify a gDNA fragment that spans heterozygous SNPs on both sides of the targeted locus (Figure 7; step 1). Correctly edited clones with evidence of biallelic amplification can be nominated for further use. Clones that appear to be correctly edited for the variant of interest but that exhibit no apparent evidence of biallelic amplification require further evaluation by an allele copy number qgPCR assay (Figure 7; step 2). Clones with significantly altered allele copy numbers should be discarded. Any clones that appear to have a normal allele copy number but that lack clear evidence of heterozygosity based on initial sequencing can be further assessed by screening for SNPs that are heterozygous in the parental line, around the targeted region using Sanger sequencing or SNP microarrays (Figure 7; step 3). Lastly, although it is more costly and requires expertise for analysis, WGS can be employed to validate correctly edited clones or even replace several QC measures, such as validation of cell line identity, genetic stability, and detection of any on-target and off-target defects.

DISCUSSION

The goal of using human iPSC lines to model monogenic or polygenic diseases is to understand how genetic variation can lead to cellular dysfunction. Owing to genetic variability between different human subjects, it has become critically important to make phenotypic comparisons within pairs of isogenic iPSC lines that differ genetically only at the intended sequence. CRISPR/Cas9 technology has enabled the generation of such controls with relative ease. However, while CRISPR/Cas9 enables precise genome editing, it can also cause significant unintended effects that may be hard to detect. In this study we focused on assessing the frequency of aberrant on-target genomic effects and alarmingly found that 33% of them had acquired on-target genetic aberrations.

both *KCNQ2-01-G6* and *KCNQ2-01-A6* clones (see Figure S9) that had appeared to be corrected by Sanger sequencing in Figure 1B. When alignments are grouped by concordance to reference assembly, partially mapped reads are displayed at the top. Reads with unmapped mates are outlined in red. Sequence alignment stops abruptly near the Cas9 cut site, with soft clipped bases and unmapped read mate sequences that are homologous to Cas9 carrying plasmid used to target this locus (see also Figure S9).

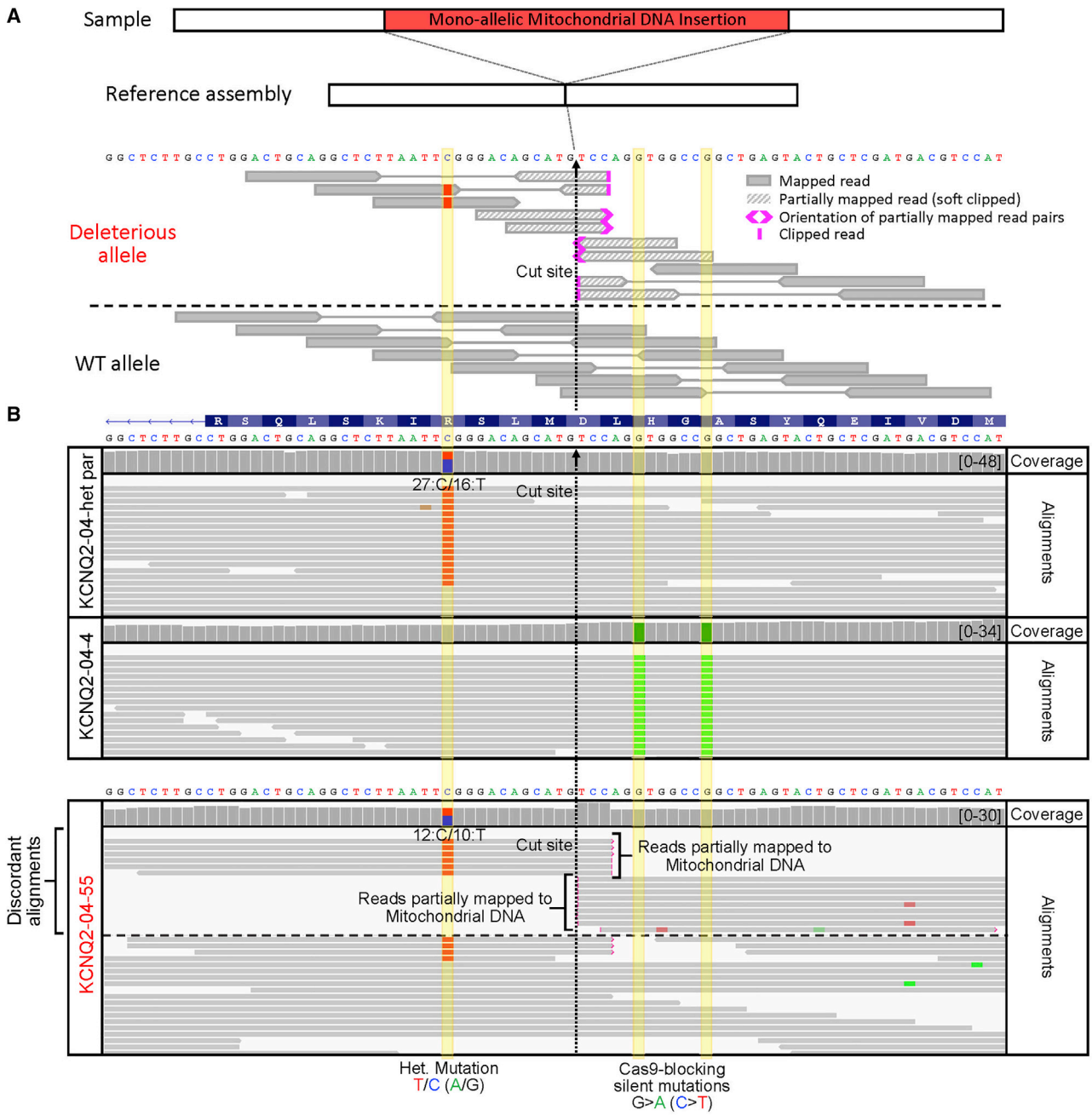

Figure 4. WGS of KCNQ2-04 clones and detection of on-target mtDNA insertion in *KCNQ2-04-55* that was falsely identified as corrected

(A) Illustration of paired-end WGS alignments in the presence of a monoallelic structural variant such as the large on-target mtDNA insertion in *KCNQ2-04-55*.

(B) WGS IGV plot showing human genome (T2T) reference assembly mapped sequencing reads around the targeted locus of *KCNQ2-04-het-parental* line, correctly edited *KCNQ2-04-4* clone, and falsely corrected *KCNQ2-04-55* clone. WGS analysis revealed the presence of the heterozygous patient mutation in *KCNQ2-04-55* clone that had appeared to be corrected by Sanger sequencing. When alignments are grouped by concordance to reference assembly, partially mapped reads are displayed at the top. Sequence alignment stops abruptly at the Cas9 cut site, with soft clipped bases and read mates from both sides corresponding to mitochondrial DNA.

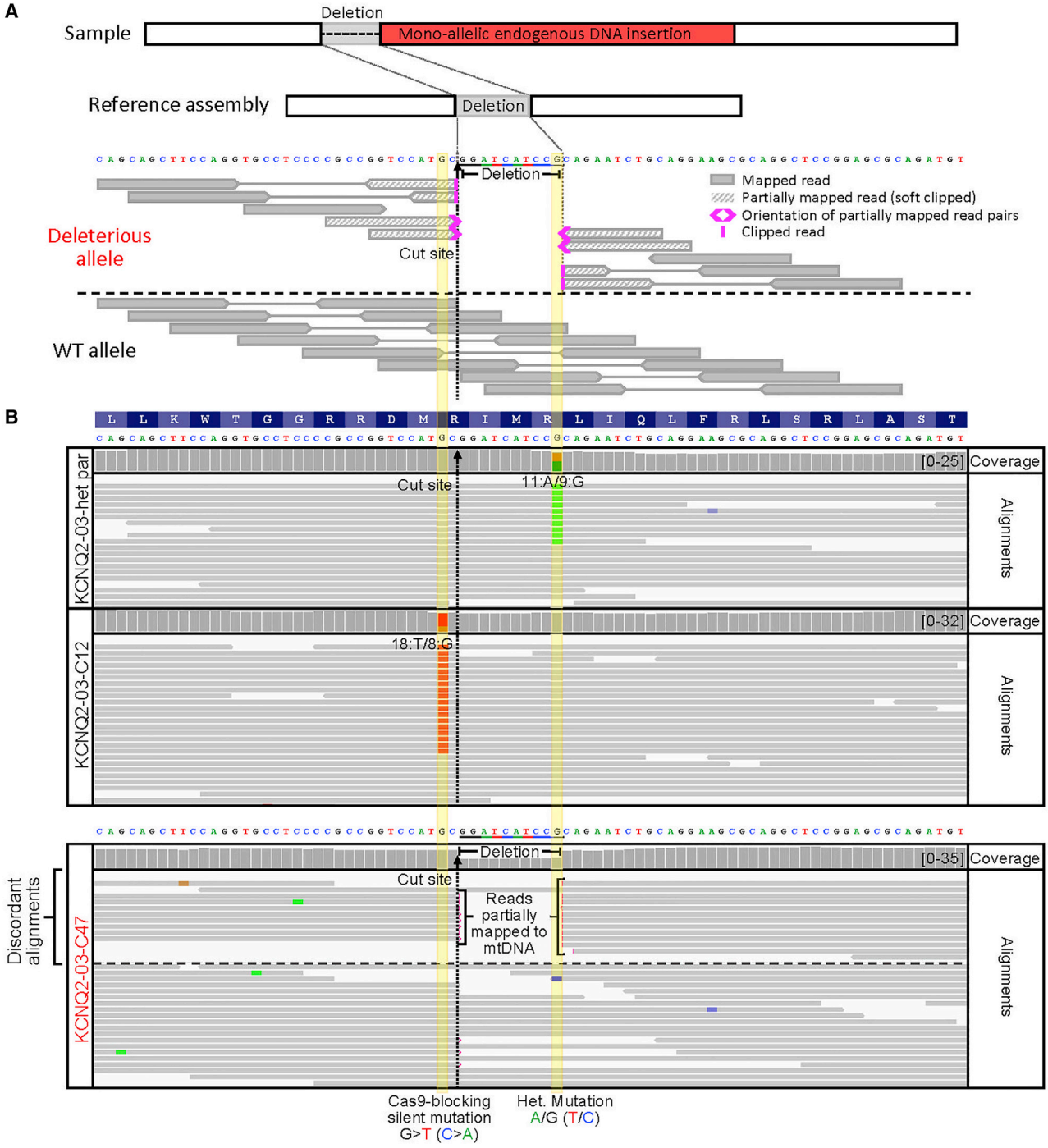

Figure 5. WGS of KCNQ2-03 clones and detection of on-target mtDNA insertion in *KCNQ2-03-C47* that was falsely identified as corrected

(A) Illustration of paired-end WGS alignments in the presence of a monoallelic structural variant such as the large on-target mitochondrial DNA insertion in *KCNQ2-03-C47*. A short 10 bp deletion was also introduced at the Cas9 cut site.

(B) WGS IGV plot showing human genome (T2T) reference assembly mapped sequencing reads around the targeted locus of *KCNQ2-03-het-parental* line, correctly edited *KCNQ2-03-C12* clone, and falsely corrected *KCNQ2-03-C47* clone. When alignments are grouped by concordance to reference assembly, partially mapped reads are displayed at the top. Sequence alignment stops abruptly at the Cas9 cut site, with soft clipped bases and read mates from both sides corresponding to mtDNA.

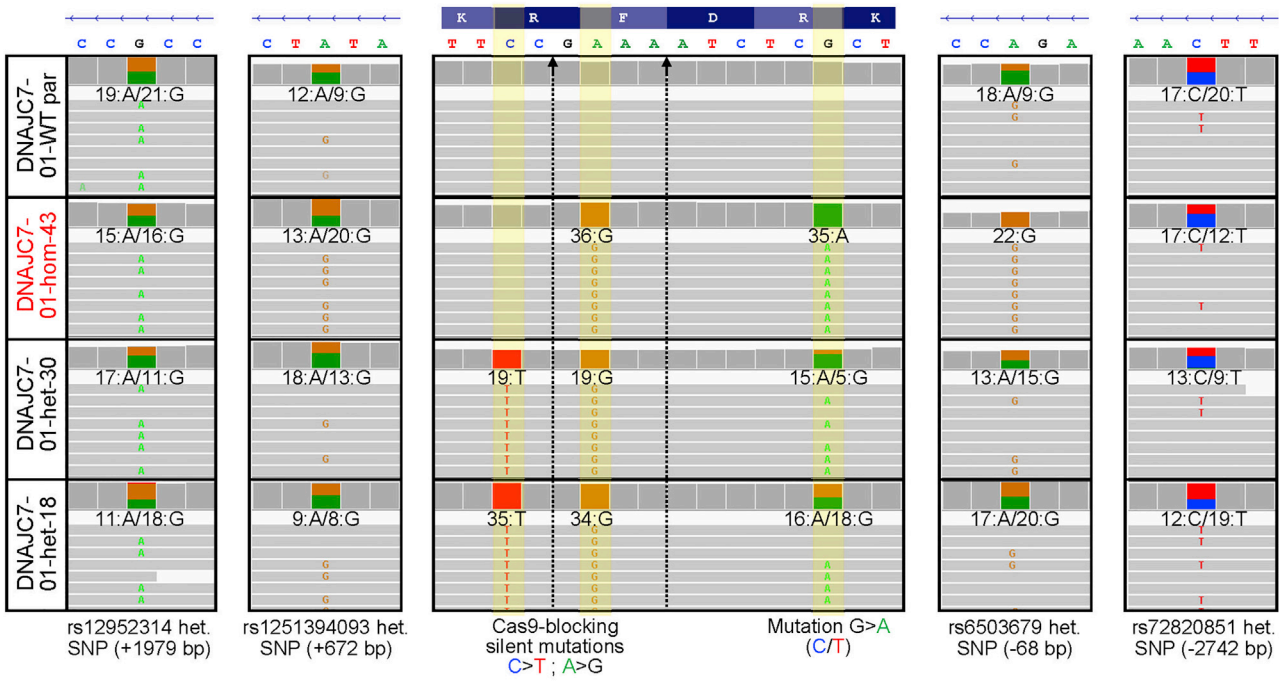

Figure 6. WGS of DNAJC7 clones and detection of heterozygous SNPs to identify copy-neutral LOH

WGS IGV plot showing human genome (T2T) reference assembly mapped sequencing reads around the targeted locus and nearby heterozygous SNPs present in *DNAJC7-01-WT-parental* line. The presence of parental line heterozygous SNPs was assessed in *DNAJC7-01-hom-43*, *DNAJC7-01-het-30*, and *DNAJC7-01-het-18* edited clones. *DNAJC7-01-hom-43* was missing a single het SNP site 68 bp from the targeted locus, while other het SNPs from both sides were still present. This indicates that copy-neutral LOH affects only this one het SNP site and not the rest of the gene.

As we demonstrate, allelic dropout leading to false identification of edited iPSC clones can severely compromise the validity of phenotyping experiments. The majority of falsely corrected clones found in our cohort had large on-target DNA insertions. The "foreign" DNA identified in 4 cases was part of the Cas9 plasmid and in 2 other cases was a large segment of mtDNA. The integration of a Cas9 plasmid gene cassette as well as parts of mtDNA has previously been reported in CRISPR/Cas9 editing systems (Bachu et al., 2015; Blondal et al., 2021; Ono et al., 2019; Strecker et al., 2019, 2020). These events are likely detrimental and can lead to haploinsufficiency or to the production of a dysfunctional protein. For example, in a recent study, a CRISPR/Cas9-edited clone was falsely identified as homozygous, while, in fact, a small deletion prevented proper sequencing of targeted region (Herai et al., 2021; Maricic et al., 2021; Trujillo et al., 2021). Moreover, the genetic consequences of copy-neutral LOH, which we identified in another falsely corrected clone, are not limited to the target locus, as LOH can uncover recessive alleles and elicit long-range transcriptional consequences. In fact, large stretches of genomic homozygosity have been identified in the normal human population and have also been associated with a large number of clinical phenotypes (Clark et al., 2019; Gibson et al., 2006; Keller et al., 2012).

The frequency of on-target defects we describe is in strong accordance with the only other comprehensive study focused on the incidence of these events in iPSCs (Weisheit et al., 2020). Weisheit et al. (2020) examined 35 iPSC clones edited across 3 genomic locations and identified on-target defects in 18%–40% of cases, whereas we examined 27 iPSC clones edited across 9 genomic locations and found defects in 33%–43% of cases. Interestingly, most defects in our cohort included large insertions (Figure S6), while the study by Weisheit et al. (2020) and several others have reported mostly large deletions (Adikusuma et al., 2018; Korablev et al., 2020; Kosicki et al., 2018; Owens et al., 2019; Yang et al., 2017). The reason for this difference is hard to discern but could be related to editing methodology or the genomic context of the targeted regions. Critically, we and Weisheit et al. highlight the difficulty in identifying on-target genomic defects by standard PCR/Sanger sequencing. Lastly, we were able to showcase the utility of WGS analysis in detecting on-target genomic defects simply by carefully examining sequence alignments. While de novo assembly strategies could be used to reconstruct the genomic sequence, we found that

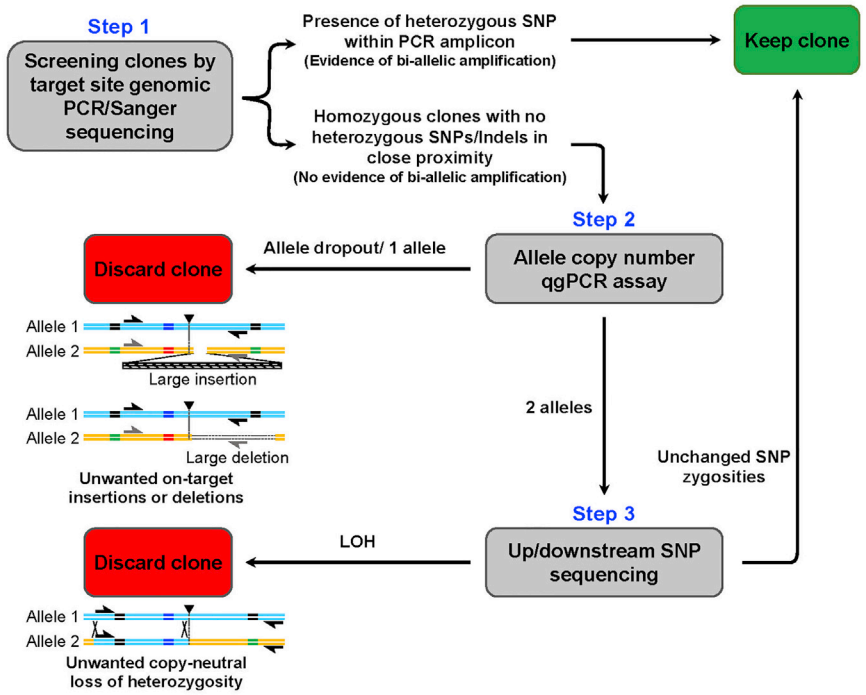

Figure 7. A cost-efficient strategy for evaluating edited iPSC lines

Steps to confirm biallelic PCR amplification and eliminate clones with unwanted on-target defects after CRISPR/Cas9 editing. PCR and Sanger sequencing of the target locus is not sufficient unless there is evidence of biallelic amplification.

careful examination of sequence alignments can be effective. Clear red flags include a sharp reduction in sequencing coverage (suggesting deletions), or a significant proportion of mapped on-target reads having mates that are only partially, or not at all mapped to the reference genome (suggesting insertions). In conclusion, we propose that it is necessary to incorporate QC strategies to detect deleterious on-target editing errors that are typically lacking in studies utilizing gene-edited iPSCs for *in vitro* disease models.

EXPERIMENTAL PROCEDURES

Detailed methods are provided in the supplemental experimental procedures

Generation, maintenance, and CRISPR/Cas9 genome editing of human iPSC lines

Patient iPSC lines were generated from PBMCs isolated from whole blood following informed consent under protocols approved both by Ann & Robert H. Lurie Children's Hospital of Chicago and Northwestern University Institutional Review Board (#2015-738) as previously described (Simkin et al., 2021). Healthy control iPSC lines CS20002 (DNAJC7-01-WT) and HPSI0114i-KOLF2 (NEK1-02-WT) were acquired from Cedar Sinai and HipSci, respectively. All iPSCs were grown on Matrigel with mTeSR1 media, maintained at 37 °C in 5% CO_2, and passaged weekly using Accutase (MilliporeSigma). The NEK1-02-WT iPSC line was edited by Jackson Laboratory. All other iPSC lines were edited by Applied StemCell Inc. (Milpitas, CA). For details on editing strategy, genomic DNA PCRs and Sanger sequencing, genomic integrity and pluripotency assays, analysis of off-target Cas9 sites, and quantitative genotyping PCR-based copy number assays, please see Supplemental experimental procedures.

Whole-genome sequencing

WGS was outsourced to Novogene Corporation Inc., as previously described (Simkin et al., 2021). We performed sequencing analysis after aligning the reads to the complete telomere-to-telomere human reference genome T2T-CHM13 v.1.1 (Nurk et al., 2021). The T2T-CHM13 reference genome improves coverage of complex regions and variant calling (Aganezov et al., 2021), delivering consensus sequences without the use of alternative contigs. IGV software was used to visualize alignment tracks and assess read coverage (Robinson et al., 2011). For details on WGS analysis, please see Supplemental experimental procedures.

Cortical neuron differentiation and Optopatch measurements

iPSCs were differentiated into glutamatergic neurons using a previously described protocol based on *Ngn2* overexpression (Simkin et al., 2021). Cryo-stocks of Ngn2 neurons differentiated from *KCNQ2-01-het parental* and *KCNQ2-01-G6* and *-A6* iPSC lines were co-plated with primary mouse glial cells onto custom-made ibidi cell culture plates. Neurons were transduced with lentiviral particles encoding all-optical electrophysiology (Optopatch) components CheRiff-BFP and QuasAr3-Citrine and recorded 2 weeks later on DIV 35 with Optopatch imaging (Hochbaum et al., 2014; Kiskinis et al., 2018; Werley et al., 2017). Additional details regarding cell culture and imaging can be found in Supplemental experimental procedures. Statistical significance was determined using t tests or Mann-Whitney tests with a custom MATLAB routine.

Statistical analysis

Statistical differences between groups were evaluated using t tests or Mann-Whitney test for nonparametric data where appropriate. All data are reported as means ± SEM.

Data availability

All data generated or analyzed during this study are included in the article and supporting files. WGS data for all patient samples are available upon request. WGS data cannot be deposited on public repositories owing to lack of patient consent.

SUPPLEMENTAL INFORMATION

Supplemental information can be found online at https://doi.org/10.1016/j.stemcr.2022.02.008.

AUTHOR CONTRIBUTIONS

Conceptualization, D.S. and E.K.; methodology, D.S. and V.P.; software, B.I.B. and S.J.L.; formal analysis, D.S., B.I.B., C.M.A, S.J.R., and V.B.; investigation: D.S., V.P., B.I.B., C.M.A., and L.A.W.; resources: J.E.L., A.L.G., and E.K.; Writing – original draft: D.S., V.P., and E.K.; Writing – review & editing: D.S., V.P., B.I.B., C.M.A., S.J.R., V.B., L.A.W., G.T.D., O.B.M., J.E.L., S.J.L., A.L.G., and E.K.; visualization: D.S., V.P., and E.K; supervision: G.T.D., O.B.M., S.J.L., A.L.G., and E.K; project administration: E.K.; funding acquisition: A.L.G. and E.K.

CONFLICT OF INTEREST

J.E.L. is a member of the scientific advisory board for Cerevel Therapeutics, is a consultant for Biogen, Inc., and provides expert testimony for Perkins Coie LLP. E.K. holds Q-State Biosciences stock. C.M.A., S.J.R., V.B., L.A.W., G.T.D., and O.B.M. are employees of Q-State Biosciences.

ACKNOWLEDGMENTS

We are grateful to the following funding sources: US National Institutes of Health (NIH) National Institute on Neurological Disorders and Stroke (NINDS) U54NS108874 (A.L.G. and E.K.), NIH/NINDS and National Institute on Aging (NIA) R01NS104219 (E.K.), NIH/NINDS R01NS073873 (J.E.L.) and R56NS073873 (J.E.L.), the Les Turner ALS Foundation (E.K.), and the New York Stem Cell Foundation (E.K.). We are grateful to Bill Skarnes and Justin McDonough for generation of the NEK1-02 iPSC isogenic line. E.K. is a Les Turner ALS Center Investigator and a New York Stem Cell Foundation – Robertson Investigator.

Received: June 4, 2021
Revised: February 3, 2022
Accepted: February 8, 2022
Published: March 10, 2022

REFERENCES

Adikusuma, F., Piltz, S., Corbett, M.A., Turvey, M., McColl, S.R., Helbig, K.J., Beard, M.R., Hughes, J., Pomerantz, R.T., and Thomas, P.Q. (2018). Large deletions induced by Cas9 cleavage. Nature *560*, E8–E9. https://doi.org/10.1038/s41586-018-0380-z.

Aganezov, S., Yan, S.M., Soto, D.C., Kirsche, M., Zarate, S., Avdeyev, P., Taylor, D.J., Shafin, K., Shumate, A., Xiao, C., et al. (2021). A complete reference genome improves analysis of human genetic variation. bioRxiv *2007*. https://doi.org/10.1101/2021.07.12.452063.

Alanis-Lobato, G., Zohren, J., McCarthy, A., Fogarty, N.M.E., Kubikova, N., Hardman, E., Greco, M., Wells, D., Turner, J.M.A., and Niakan, K.K. (2021). Frequent loss of heterozygosity in CRISPR-Cas9-edited early human embryos. Proc. Natl. Acad. Sci. United States America *118*, 202004832. https://doi.org/10.1073/pnas.2004832117.

Alateeq, S., Ovchinnikov, D., Tracey, T., Whitworth, D., Al-Rubaish, A., Al-Ali, A., and Wolvetang, E. (2018). Identification of on-target mutagenesis during correction of a beta-thalassemia splice mutation in iPS cells with optimised CRISPR/Cas9-double nickase reveals potential safety concerns. APL Bioeng. *2*, 046103. https://doi.org/10.1063/1.5048625.

Bachu, R., Bergareche, I., and Chasin, L.A. (2015). CRISPR-Cas targeted plasmid integration into mammalian cells via non-homologous end joining. Biotechnol. Bioeng. *112*, 2154–2162. https://doi.org/10.1002/bit.25629.

Bibikova, M., Beumer, K., Trautman, J.K., and Carroll, D. (2003). Enhancing gene targeting with designed zinc finger nucleases. Sci. (New York, N.Y *300*, 764. https://doi.org/10.1126/science.1079512.

Blair, J.D., Bateup, H.S., and Hockemeyer, D.F. (2016). Establishment of genome-edited human pluripotent stem cell lines: from targeting to isolation. J. visualized experiments : JoVE, e53583. https://doi.org/10.3791/53583.

Blondal, T., Gamba, C., Moller Jagd, L., Su, L., Demirov, D., Guo, S., Johnston, C.M., Riising, E.M., Wu, X., Mikkelsen, M.J., et al. (2021). Verification of CRISPR editing and finding transgenic inserts by Xdrop indirect sequence capture followed by short- and long-read sequencing. Methods *191*, 68–77. https://doi.org/10.1016/j.ymeth.2021.02.003.

Byrne, S.M., Mali, P., and Church, G.M. (2014). Genome editing in human stem cells. Methods Enzymol. *546*, 119–138. https://doi.org/10.1016/B978-0-12-801185-0.00006-4.

Cho, S.W., Kim, S., Kim, Y., Kweon, J., Kim, H.S., Bae, S., and Kim, J.S. (2014). Analysis of off-target effects of CRISPR/Cas-derived RNA-guided endonucleases and nickases. Genome Res. *24*, 132–141. https://doi.org/10.1101/gr.162339.113.

Clark, D.W., Okada, Y., Moore, K.H.S., Mason, D., Pirastu, N., Gandin, I., Mattsson, H., Barnes, C.L.K., Lin, K., Zhao, J.H., et al. (2019). Associations of autozygosity with a broad range of human phenotypes. Nat. Commun. *10*, 4957. https://doi.org/10.1038/s41467-019-12283-6.

Dhindsa, R.S., Copeland, B.R., Mustoe, A.M., and Goldstein, D.B. (2020). Natural selection shapes codon usage in the human genome. Am. J. Hum. Genet. *107*, 83–95. https://doi.org/10.1016/j.ajhg.2020.05.011.

Fu, Y., Foden, J.A., Khayter, C., Maeder, M.L., Reyon, D., Joung, J.K., and Sander, J.D. (2013). High-frequency off-target mutagenesis

induced by CRISPR-Cas nucleases in human cells. Nat. Biotechnol. *31*, 822–826. https://doi.org/10.1038/nbt.2623.

Fu, Y.W., Dai, X.Y., Wang, W.T., Yang, Z.X., Zhao, J.J., Zhang, J.P., Wen, W., Zhang, F., Oberg, K.C., Zhang, L., et al. (2021). Dynamics and competition of CRISPR-Cas9 ribonucleoproteins and AAV donor-mediated NHEJ, MMEJ and HDR editing. Nucleic Acids Res. *49*, 969–985. https://doi.org/10.1093/nar/gkaa1251.

Gibson, J., Morton, N.E., and Collins, A. (2006). Extended tracts of homozygosity in outbred human populations. Hum. Mol. Genet. *15*, 789–795. https://doi.org/10.1093/hmg/ddi493.

Gorter de Vries, A.R., Couwenberg, L.G.F., van den Broek, M., de la Torre Cortes, P., Ter Horst, J., Pronk, J.T., and Daran, J.G. (2019). Allele-specific genome editing using CRISPR-Cas9 is associated with loss of heterozygosity in diploid yeast. Nucleic Acids Res. *47*, 1362–1372. https://doi.org/10.1093/nar/gky1216.

Hajiahmadi, Z., Movahedi, A., Wei, H., Li, D., Orooji, Y., Ruan, H., and Zhuge, Q. (2019). Strategies to increase on-target and reduce off-target effects of the CRISPR/Cas9 system in plants. Int. J. Mol. Sci. *20*. https://doi.org/10.3390/ijms20153719.

Herai, R.H., Szeto, R.A., Trujillo, C.A., and Muotri, A.R. (2021). Response to Comment on "Reintroduction of the archaic variant of NOVA1 in cortical organoids alters neurodevelopment". Science *374*, eabi9881. https://doi.org/10.1126/science.abi9881.

Hochbaum, D.R., Zhao, Y., Farhi, S.L., Klapoetke, N., Werley, C.A., Kapoor, V., Zou, P., Kralj, J.M., Maclaurin, D., Smedemark-Margulies, N., et al. (2014). All-optical electrophysiology in mammalian neurons using engineered microbial rhodopsins. Nat. Methods *11*, 825–833. https://doi.org/10.1038/nmeth.3000.

Hockemeyer, D., and Jaenisch, R. (2016). Induced pluripotent stem cells meet genome editing. Cell Stem Cell *18*, 573–586. https://doi.org/10.1016/j.stem.2016.04.013.

Hsu, P.D., Scott, D.A., Weinstein, J.A., Ran, F.A., Konermann, S., Agarwala, V., Li, Y., Fine, E.J., Wu, X., Shalem, O., et al. (2013). DNA targeting specificity of RNA-guided Cas9 nucleases. Nat. Biotechnol. *31*, 827–832. https://doi.org/10.1038/nbt.2647.

Ichida, J.K., and Kiskinis, E. (2015). Probing disorders of the nervous system using reprogramming approaches. EMBO J. *34*, 1456–1477. https://doi.org/10.15252/embj.201591267.

Ikeda, K., Uchida, N., Nishimura, T., White, J., Martin, R.M., Nakauchi, H., Sebastiano, V., Weinberg, K.I., and Porteus, M.H. (2018). Efficient scarless genome editing in human pluripotent stem cells. Nat. Methods *15*, 1045–1047. https://doi.org/10.1038/s41592-018-0212-y.

Keller, M.C., Simonson, M.A., Ripke, S., Neale, B.M., Gejman, P.V., Howrigan, D.P., Lee, S.H., Lencz, T., Levinson, D.F., Sullivan, P.F., et al. (2012). Runs of homozygosity implicate autozygosity as a schizophrenia risk factor. Plos Genet. *8*, e1002656. https://doi.org/10.1371/journal.pgen.1002656.

Kiskinis, E., Kralj, J.M., Zou, P., Weinstein, E.N., Zhang, H., Tsioras, K., Wiskow, O., Ortega, J.A., Eggan, K., and Cohen, A.E. (2018). All-optical electrophysiology for high-throughput functional characterization of a human iPSC-derived motor neuron model of ALS. Stem Cell Rep. *10*, 1991–2004. https://doi.org/10.1016/j.stemcr.2018.04.020.

Korablev, A., Lukyanchikova, V., Serova, I., and Battulin, N. (2020). On-target CRISPR/Cas9 activity can cause undesigned large deletion in mouse zygotes. Int. J. Mol. Sci. *21*. https://doi.org/10.3390/ijms21103604.

Kosicki, M., Tomberg, K., and Bradley, A. (2018). Repair of double-strand breaks induced by CRISPR-Cas9 leads to large deletions and complex rearrangements. Nat. Biotechnol. *36*, 765–771. https://doi.org/10.1038/nbt.4192.

Kwart, D., Paquet, D., Teo, S., and Tessier-Lavigne, M. (2017). Precise and efficient scarless genome editing in stem cells using CORRECT. Nat. Protoc. *12*, 329–354. https://doi.org/10.1038/nprot.2016.171.

Ledford, H. (2020). CRISPR gene editing in human embryos wreaks chromosomal mayhem. Nature *583*, 17–18. https://doi.org/10.1038/d41586-020-01906-4.

Leibowitz, M.L., Papathanasiou, S., Doerfler, P.A., Blaine, L.J., Sun, L., Yao, Y., Zhang, C.Z., Weiss, M.J., and Pellman, D. (2021). Chromothripsis as an on-target consequence of CRISPR-Cas9 genome editing. Nat. Genet. *53*, 895–905. https://doi.org/10.1038/s41588-021-00838-7.

Liang, D., Gutierrez, N.M., Chen, T., Lee, Y., Park, S.-W., Ma, H., Koski, A., Ahmed, R., Darby, H., Li, Y., et al. (2020). Frequent Gene Conversion in Human Embryos Induced by Double Strand Breaks. bioRxiv *2006*. https://doi.org/10.1101/2020.06.19.162214.

Liang, F., Han, M., Romanienko, P.J., and Jasin, M. (1998). Homology-directed repair is a major double-strand break repair pathway in mammalian cells. Proc. Natl. Acad. Sci. U S A *95*, 5172–5177. https://doi.org/10.1073/pnas.95.9.5172.

Ma, H., Marti-Gutierrez, N., Park, S.W., Wu, J., Lee, Y., Suzuki, K., Koski, A., Ji, D., Hayama, T., Ahmed, R., et al. (2017). Correction of a pathogenic gene mutation in human embryos. Nature *548*, 413–419. https://doi.org/10.1038/nature23305.

Maguire, J.A., Cardenas-Diaz, F.L., Gadue, P., and French, D.L. (2019). Highly efficient CRISPR-cas9-mediated genome editing in human pluripotent stem cells. Curr. Protoc. Stem Cell Biol *48*, e64. https://doi.org/10.1002/cpsc.64.

Mao, Z., Bozzella, M., Seluanov, A., and Gorbunova, V. (2008). Comparison of nonhomologous end joining and homologous recombination in human cells. DNA Repair (Amst) *7*, 1765–1771. https://doi.org/10.1016/j.dnarep.2008.06.018.

Maricic, T., Helmbrecht, N., Riesenberg, S., Macak, D., Kanis, P., Lackner, M., Pugach-Matveeva, A.D., and Paabo, S. (2021). Comment on "Reintroduction of the archaic variant of NOVA1 in cortical organoids alters neurodevelopment". Science *374*, eabi6060. https://doi.org/10.1126/science.abi6060.

Martin, R.M., Ikeda, K., Cromer, M.K., Uchida, N., Nishimura, T., Romano, R., Tong, A.J., Lemgart, V.T., Camarena, J., Pavel-Dinu, M., et al. (2019). Highly efficient and marker-free genome editing of human pluripotent stem cells by CRISPR-cas9 RNP and AAV6 donor-mediated homologous recombination. Cell Stem Cell *24*, 821–828.e825. https://doi.org/10.1016/j.stem.2019.04.001.

Merkle, F.T., and Eggan, K. (2013). Modeling human disease with pluripotent stem cells: from genome association to function. Cell

Stem Cell *12*, 656–668. https://doi.org/10.1016/j.stem.2013.05.016.

Merkle, F.T., Neuhausser, W.M., Santos, D., Valen, E., Gagnon, J.A., Maas, K., Sandoe, J., Schier, A.F., and Eggan, K. (2015). Efficient CRISPR-Cas9-mediated generation of knockin human pluripotent stem cells lacking undesired mutations at the targeted locus. Cell Rep *11*, 875–883. https://doi.org/10.1016/j.celrep.2015.04.007.

Mianne, J., Bourguignon, C., Nguyen Van, C., Fieldes, M., Nasri, A., Assou, S., and De Vos, J. (2020). Pipeline for the generation and characterization of transgenic human pluripotent stem cells using the CRISPR/Cas9 technology. Cells 9. https://doi.org/10.3390/cells9051312.

Nurk, S., Koren, S., Rhie, A., Rautiainen, M., Bzikadze, A.V., Mikheenko, A., Vollger, M.R., Altemose, N., Uralsky, L., Gershman, A., et al. (2021). The complete sequence of a human genome. bioRxiv *2005*. https://doi.org/10.1101/2021.05.26.445798.

O'Keefe, C., McDevitt, M.A., and Maciejewski, J.P. (2010). Copy neutral loss of heterozygosity: a novel chromosomal lesion in myeloid malignancies. Blood *115*, 2731–2739. https://doi.org/10.1182/blood-2009-10-201848.

Okamoto, S., Amaishi, Y., Maki, I., Enoki, T., and Mineno, J. (2019). Highly efficient genome editing for single-base substitutions using optimized ssODNs with Cas9-RNPs. Sci. Rep. *9*, 4811. https://doi.org/10.1038/s41598-019-41121-4.

Ono, R., Yasuhiko, Y., Aisaki, K.I., Kitajima, S., Kanno, J., and Hirabayashi, Y. (2019). Exosome-mediated horizontal gene transfer occurs in double-strand break repair during genome editing. Commun. Biol. *2*, 57. https://doi.org/10.1038/s42003-019-0300-2.

Owens, D.D.G., Caulder, A., Frontera, V., Harman, J.R., Allan, A.J., Bucakci, A., Greder, L., Codner, G.F., Hublitz, P., McHugh, P.J., et al. (2019). Microhomologies are prevalent at Cas9-induced larger deletions. Nucleic Acids Res. *47*, 7402–7417. https://doi.org/10.1093/nar/gkz459.

Paquet, D., Kwart, D., Chen, A., Sproul, A., Jacob, S., Teo, S., Olsen, K.M., Gregg, A., Noggle, S., and Tessier-Lavigne, M. (2016). Efficient introduction of specific homozygous and heterozygous mutations using CRISPR/Cas9. Nature *533*, 125–129. https://doi.org/10.1038/nature17664.

Pattanayak, V., Lin, S., Guilinger, J.P., Ma, E., Doudna, J.A., and Liu, D.R. (2013). High-throughput profiling of off-target DNA cleavage reveals RNA-programmed Cas9 nuclease specificity. Nat. Biotechnol. *31*, 839–843. https://doi.org/10.1038/nbt.2673.

Popp, B., Krumbiegel, M., Grosch, J., Sommer, A., Uebe, S., Kohl, Z., Plotz, S., Farrell, M., Trautmann, U., Kraus, C., et al. (2018). Need for high-resolution genetic analysis in iPSC: results and lessons from the ForIPS consortium. Sci. Rep. *8*, 17201. https://doi.org/10.1038/s41598-018-35506-0.

Prat, F., Toutain, J., Boutin, J., Amintas, S., Cullot, G., Lalanne, M., Lamrissi-Garcia, I., Moranvillier, I., Richard, E., Blouin, J.M., et al. (2020). Mutation-specific guide RNA for compound heterozygous porphyria on-target scarless correction by CRISPR/Cas9 in stem cells. Stem Cell Rep. *15*, 677–693. https://doi.org/10.1016/j.stemcr.2020.07.015.

Przewrocka, J., Rowan, A., Rosenthal, R., Kanu, N., and Swanton, C. (2020). Unintended on-target chromosomal instability following CRISPR/Cas9 single gene targeting. Ann. Oncol. *31*, 1270–1273. https://doi.org/10.1016/j.annonc.2020.04.480.

Rayner, E., Durin, M.A., Thomas, R., Moralli, D., O'Cathail, S.M., Tomlinson, I., Green, C.M., and Lewis, A. (2019). CRISPR-Cas9 causes chromosomal instability and rearrangements in cancer cell lines, detectable by cytogenetic methods. CRISPR J. *2*, 406–416. https://doi.org/10.1089/crispr.2019.0006.

Robinson, J.T., Thorvaldsdottir, H., Winckler, W., Guttman, M., Lander, E.S., Getz, G., and Mesirov, J.P. (2011). Integrative genomics viewer. Nat. Biotechnol. *29*, 24–26. https://doi.org/10.1038/nbt.1754.

Sander, J.D., and Joung, J.K. (2014). CRISPR-Cas systems for editing, regulating and targeting genomes. Nat. Biotechnol. *32*, 347–355. https://doi.org/10.1038/nbt.2842.

Santos, D.P., Kiskinis, E., Eggan, K., and Merkle, F.T. (2016). Comprehensive protocols for CRISPR/Cas9-based gene editing in human pluripotent stem cells. Curr. Protoc. Stem Cell Biol *38*, 5B 6 1–5B 6 60. https://doi.org/10.1002/cpsc.15.

Shestak, A.G., Bukaeva, A.A., Saber, S., and Zaklyazminskaya, E.V. (2021). Allelic dropout is a common phenomenon that reduces the diagnostic yield of PCR-based sequencing of targeted gene panels. Front Genet. *12*, 620337. https://doi.org/10.3389/fgene.2021.620337.

Shin, H.Y., Wang, C., Lee, H.K., Yoo, K.H., Zeng, X., Kuhns, T., Yang, C.M., Mohr, T., Liu, C., and Hennighausen, L. (2017). CRISPR/Cas9 targeting events cause complex deletions and insertions at 17 sites in the mouse genome. Nat. Commun. *8*, 15464. https://doi.org/10.1038/ncomms15464.

Shrivastav, M., De Haro, L.P., and Nickoloff, J.A. (2008). Regulation of DNA double-strand break repair pathway choice. Cell Res *18*, 134–147. https://doi.org/10.1038/cr.2007.111.

Simkin, D., Marshall, K.A., Vanoye, C.G., Desai, R.R., Bustos, B.I., Piyevsky, B.N., Ortega, J.A., Forrest, M., Robertson, G.L., Penzes, P., et al. (2021). Dyshomeostatic modulation of Ca(2+)-activated K(+) channels in a human neuronal model of KCNQ2 encephalopathy. Elife *10*, e64434. https://doi.org/10.7554/eLife.64434.

Steeg, R., Mueller, S.C., Mah, N., Holst, B., Cabrera-Socorro, A., Stacey, G.N., De Sousa, P.A., Courtney, A., and Zimmermann, H. (2021). EBiSC best practice: how to ensure optimal generation, qualification, and distribution of iPSC lines. Stem Cell Rep. *16*, 1853–1867. https://doi.org/10.1016/j.stemcr.2021.07.009.

Steyer, B., Bu, Q., Cory, E., Jiang, K., Duong, S., Sinha, D., Steltzer, S., Gamm, D., Chang, Q., and Saha, K. (2018). Scarless genome editing of human pluripotent stem cells via transient puromycin selection. Stem Cell Rep. *10*, 642–654. https://doi.org/10.1016/j.stemcr.2017.12.004.

Strecker, J., Ladha, A., Gardner, Z., Schmid-Burgk, J.L., Makarova, K.S., Koonin, E.V., and Zhang, F. (2019). RNA-guided DNA insertion with CRISPR-associated transposases. Science *365*, 48–53. https://doi.org/10.1126/science.aax9181.

Strecker, J., Ladha, A., Makarova, K.S., Koonin, E.V., and Zhang, F. (2020). Response to Comment on "RNA-Guided DNA Insertion with CRISPR-Associated Transposases". Science *368*. https://doi.org/10.1126/science.abb2920.

Trujillo, C.A., Rice, E.S., Schaefer, N.K., Chaim, I.A., Wheeler, E.C., Madrigal, A.A., Buchanan, J., Preissl, S., Wang, A., Negraes, P.D., et al. (2021). Reintroduction of the archaic variant of NOVA1 in cortical organoids alters neurodevelopment. Science *371*. https://doi.org/10.1126/science.aax2537.

Van der Auwera, G.A., Carneiro, M.O., Hartl, C., Poplin, R., Del Angel, G., Levy-Moonshine, A., Jordan, T., Shakir, K., Roazen, D., Thibault, J., et al. (2013). From FastQ data to high confidence variant calls: the Genome Analysis Toolkit best practices pipeline. Curr. Protoc. Bioinformatics *43*, 11. 11 10 33. https://doi.org/10.1002/0471250953.bi1110s43.

Van der Auwera, G.A., and O'Connor, B.D. (2020). Genomics in the Cloud: Using Docker, GATK, and WDL in Terra (O'Reilly Media).

Wang, H., and Xu, X. (2017). Microhomology-mediated end joining: new players join the team. Cell Biosci *7*, 6. https://doi.org/10.1186/s13578-017-0136-8.

Wang, Y., Liu, K.I., Sutrisnoh, N.B., Srinivasan, H., Zhang, J., Li, J., Zhang, F., Lalith, C.R.J., Xing, H., Shanmugam, R., et al. (2018). Systematic evaluation of CRISPR-Cas systems reveals design principles for genome editing in human cells. Genome Biol. *19*, 62. https://doi.org/10.1186/s13059-018-1445-x.

Weisheit, I., Kroeger, J.A., Malik, R., Klimmt, J., Crusius, D., Dannert, A., Dichgans, M., and Paquet, D. (2020). Detection of deleterious on-target effects after HDR-mediated CRISPR editing. Cell Rep *31*, 107689. https://doi.org/10.1016/j.celrep.2020.107689.

Weisheit, I., Kroeger, J.A., Malik, R., Wefers, B., Lichtner, P., Wurst, W., Dichgans, M., and Paquet, D. (2021). Simple and reliable detection of CRISPR-induced on-target effects by qgPCR and SNP genotyping. Nat. Protoc. *16*, 1714–1739. https://doi.org/10.1038/s41596-020-00481-2.

Werley, C.A., Brookings, T., Upadhyay, H., Williams, L.A., McManus, O.B., and Dempsey, G.T. (2017). All-optical electrophysiology for disease modeling and pharmacological characterization of neurons. Curr. Protoc. Pharmacol. *78*, 11. 11 20 24. https://doi.org/10.1002/cpph.25.

Yang, Y.J., Wang, Y., Li, Z.F., Gong, Y., Zhang, P., Hu, W.C., Sheng, D.H., and Li, Y.Z. (2017). Increasing on-target cleavage efficiency for CRISPR/Cas9-induced large fragment deletion in Myxococcus xanthus. Microb. Cell Fact *16*, 142. https://doi.org/10.1186/s12934-017-0758-x.

Zischewski, J., Fischer, R., and Bortesi, L. (2017). Detection of on-target and off-target mutations generated by CRISPR/Cas9 and other sequence-specific nucleases. Biotechnol. Adv. *35*, 95–104. https://doi.org/10.1016/j.biotechadv.2016.12.003.

Zuccaro, M.V., Xu, J., Mitchell, C., Marin, D., Zimmerman, R., Rana, B., Weinstein, E., King, R.T., Palmerola, K.L., Smith, M.E., et al. (2020). Allele-specific chromosome removal after Cas9 cleavage in human embryos. Cell *183*, 1650–1664.e1615. https://doi.org/10.1016/j.cell.2020.10.025.

Stem Cell Reports, Volume *17*

Supplemental Information

Homozygous might be hemizygous: CRISPR/Cas9 editing in iPSCs results in detrimental on-target defects that escape standard quality controls

Dina Simkin, Vasileios Papakis, Bernabe I. Bustos, Christina M. Ambrosi, Steven J. Ryan, Valeriya Baru, Luis A. Williams, Graham T. Dempsey, Owen B. McManus, John E. Landers, Steven J. Lubbe, Alfred L. George Jr., and Evangelos Kiskinis

SUPPLEMENTAL INFORMATION

SUPPLEMENTAL FIGURES

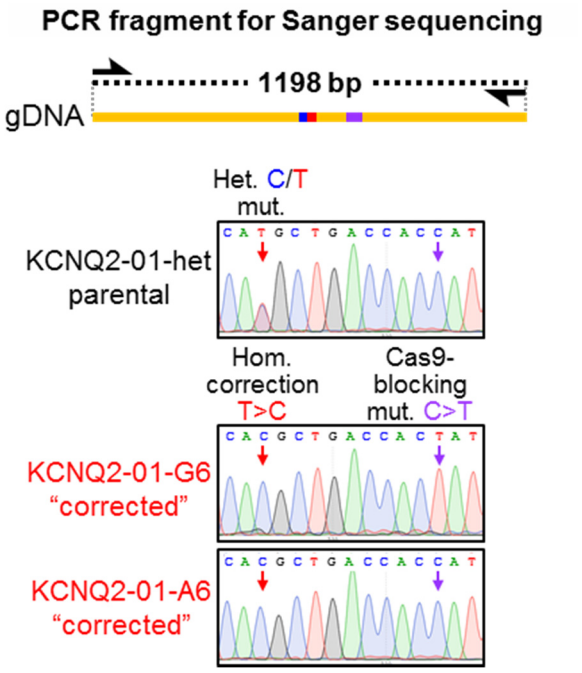

Figure S1. PCR and Sanger sequencing of target locus. Related to Figure 1. PCR amplification of 1198 bp spanning the target locus and Sanger sequencing.

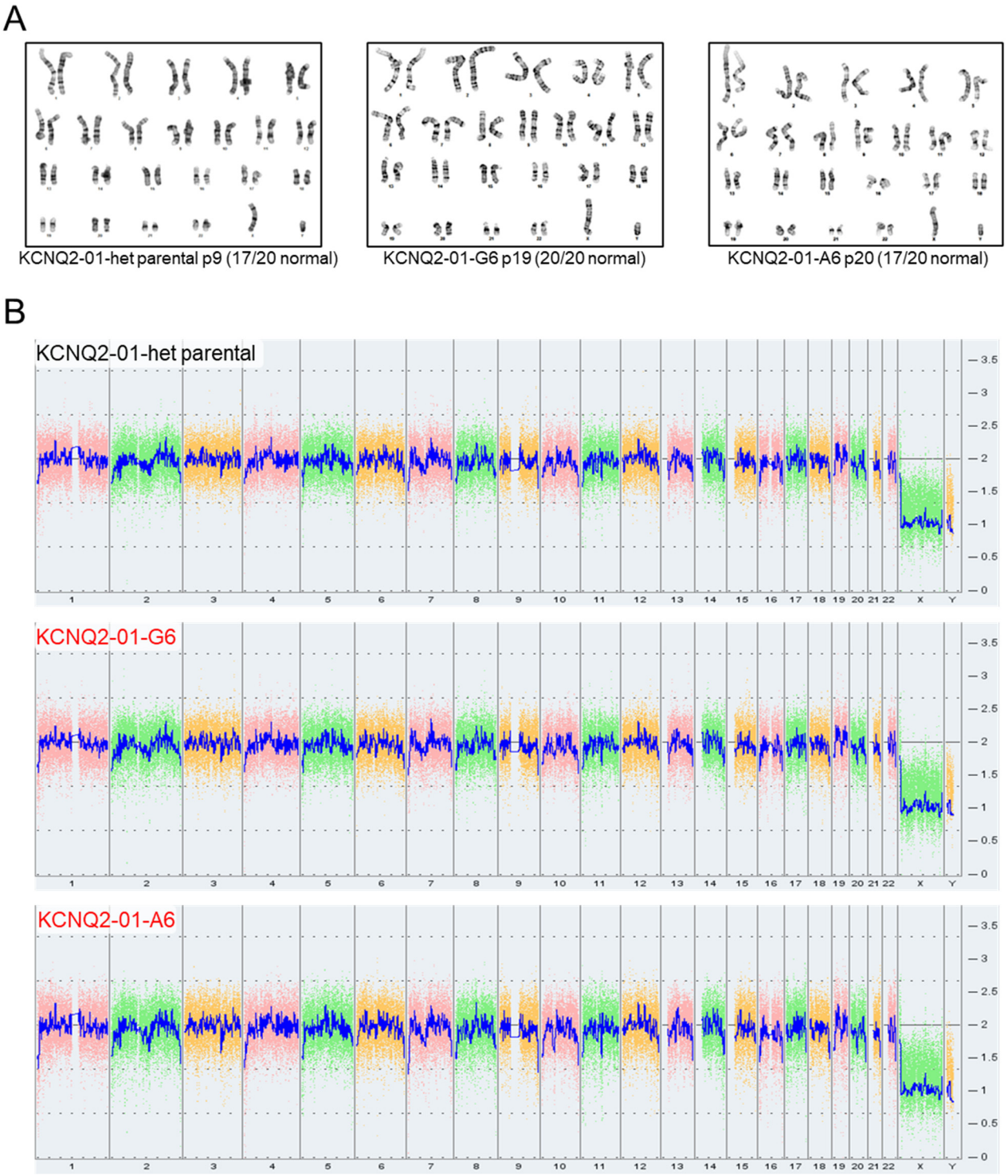

Figure S2. iPSC QCs. Related to Figure 1. (A) G-band karyotype analysis of *KCNQ2-01-het parental* and CRISPR/Cas9 edited clones *KCNQ2-01-G6* and *KCNQ2-01-A6* revealed normal karyotypes. (B) Karyostat digital karyotype analysis revealed no larger genomic aberrations.

A

DNA STR profile fingerprint analysis summary

	D3S1358	THO1	D21S11	D18S51	Penta E
KCNQ2-01-het parental	14,18	9,9.3	29	15	11,12
KCNQ2-01-G6	14,18	9,9.3	29	15	11,12
KCNQ2-01-A6	14,18	9,9.3	29	15	11,12

	D5S818	D13S317	D7S820	D16S539	CSF1PO	Penta D
KCNQ2-01-het parental	11,13	11,12	8,12	10,13	9,14	9
KCNQ2-01-G6	11,13	11,12	8,12	10,13	9,14	9
KCNQ2-01-A6	11,13	11,12	8,12	10,13	9,14	9

	Amelogenin	vWA	D8S1179	TPOX	FGA
KCNQ2-01-het parental	X,Y	15,19	11,16	8	21,22.2
KCNQ2-01-G6	X,Y	15,19	11,16	8	21,22.2
KCNQ2-01-A6	X,Y	15,19	11,16	8	21,22.2

B

KCNQ2-01-het parental

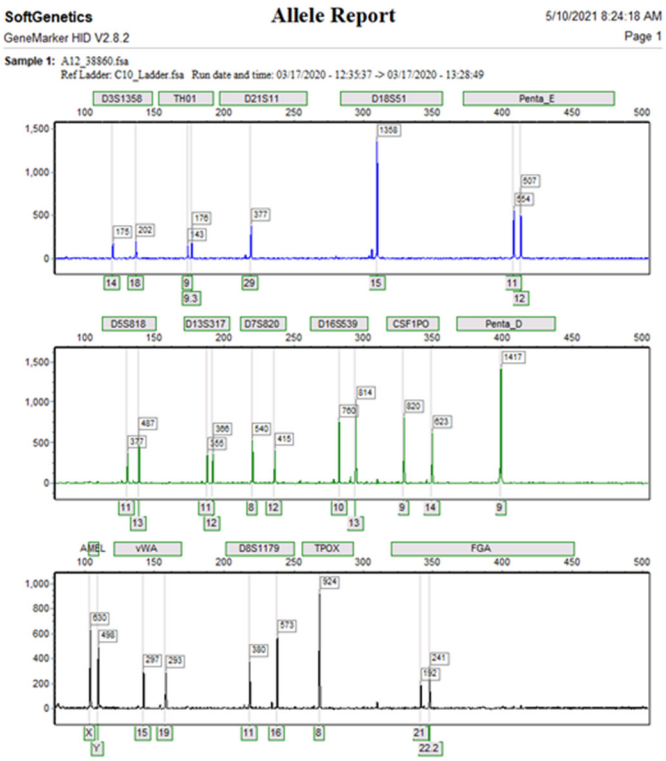

KCNQ2-01-G6

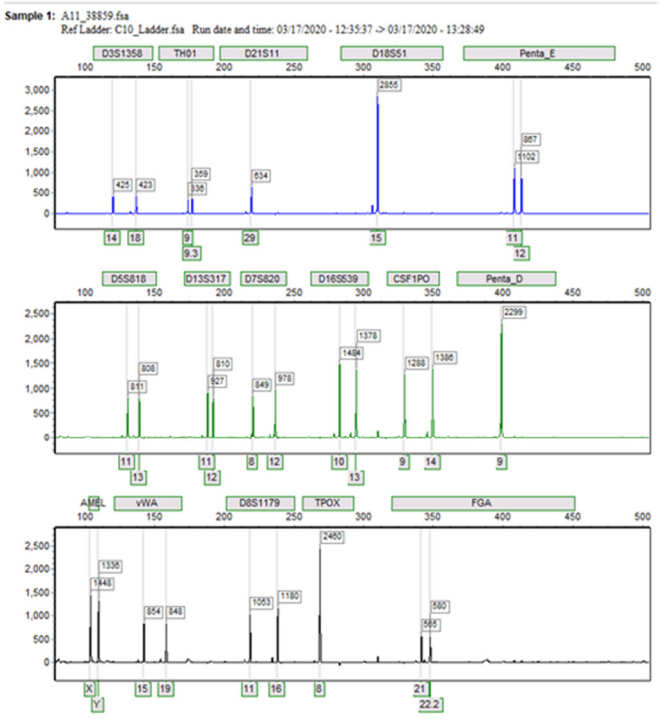

KCNQ2-01-A6

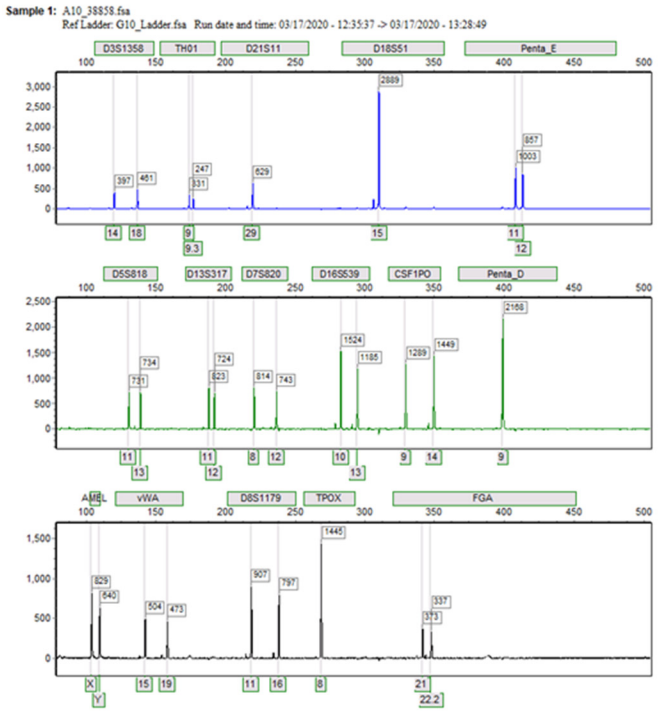

Figure S3. iPSC QCs. Related to Figure 1. DNA short tandem repeat (STR) profile analysis revealed that all 3 iPSC clones came from the same individual. (A) DNA STR profile of cell line *KCNQ2-01-het parental* is consistent

with the presence of a single cell line. The alleles match the DNA STR profile of iPSC samples *KCNQ2-01-G6* and *KCNQ2-01-A6*. The alleles do not match the DNA STR profile of the cell lines published in the ATCC, NIH, or DSMZ databases. Tables summarize the peaks of the electropherograms for each SNP for the three iPSC lines. (B) Electropherograms with peaks for alleles which are specified above each peak, outlined in green.

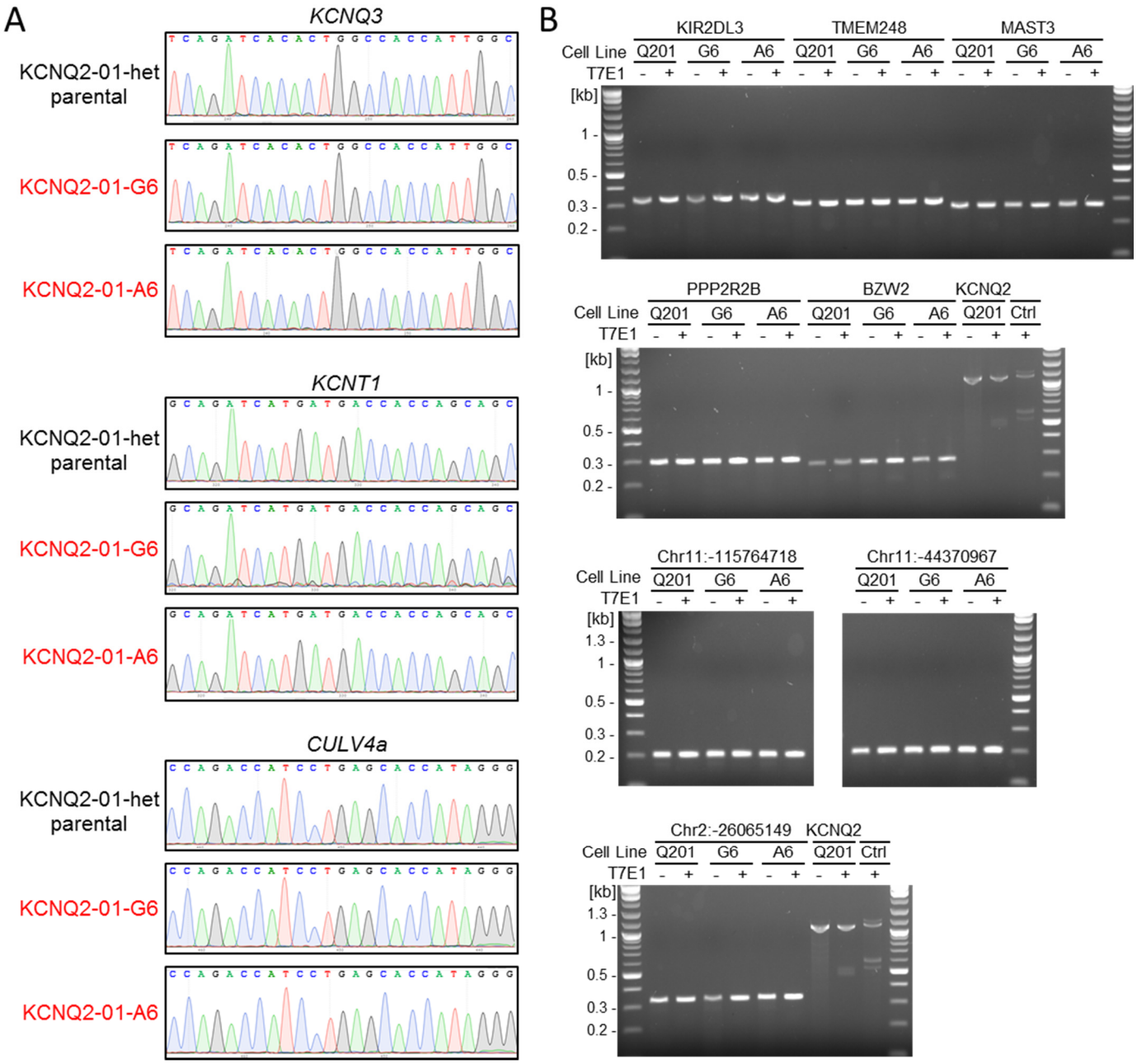

Figure S4. iPSC CRISPR/Cas9 off-target analysis. Related to Figure 1. Analysis of potential CRISPR off-target sites. CCTop CRISPR/Cas9 off-target online predictor was used to predict genomic regions of homology with the sgRNA sequence used for CRISPR/Cas9 targeting (Table S3). (A) The top 11 off-target sites were chosen of which only three (*KCNQ3*, *KCNT1* and *CULV4A*) were in exonic regions. PCR amplification and Sanger sequencing of 800-1000 bp surrounding these off-target regions revealed no deviation of sequence in these regions in the edited clones from the parental untargeted line. (B) Eight other intronic and intergenic regions were analyzed by PCR amplification of 200-300 bp fragments and a T7 endonuclease digestion assay. PCR fragments without (-) and with (+) T7 endonuclease treatment were run on an 2% agarose gel for each sample and for each off-target region. No mutations affecting a single allele were identified. A control sample was run using a 1.2 kb PCR fragment that contained the patient single bp heterozygous mutation of *KCNQ2* before and after T7E1 digestion. Doublet bands are visible in the gel suggesting that a single bp heterozygous mutation would be detectable with this assay.

A

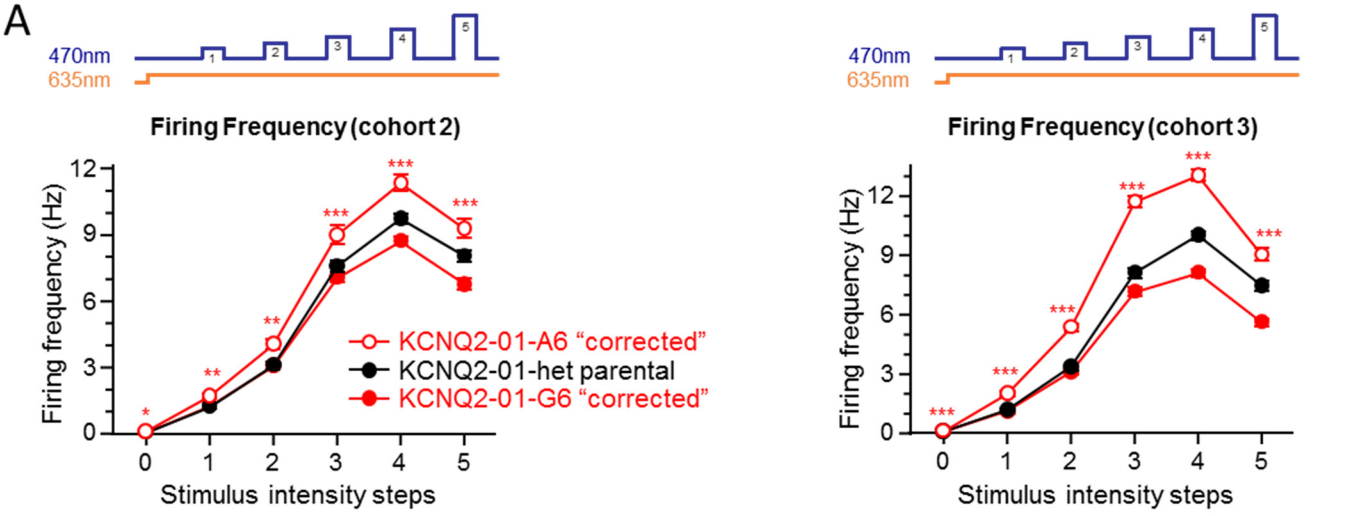

B

Max
Min

Parameters	Optopatch Cohort 1 (same as Figure 1D)			Optopatch Cohort 2			Optopatch Cohort 3		
	KCNQ2-01-A6	KCNQ2-01-het par	KCNQ2-01-G6	KCNQ2-01-A6	KCNQ2-01-het par	KCNQ2-01-G6	KCNQ2-01-A6	KCNQ2-01-het par	KCNQ2-01-G6
Spike Max Derivative	0.240±0.002	0.242±0.002	0.245±0.002	0.256±0.002	0.259±0.002	0.264±0.003	0.248±0.002***	0.260±0.002	0.262±0.002
Spike Rise Time (ms)	4.98±0.05**	4.91±0.04	4.77±0.05	4.61±0.05**	4.50±0.04	4.40±0.04	4.82±0.04***	4.53±0.04	4.42±0.04
AHP (normalized fluorescence)	-0.38±0.33***	-0.40±0.53	-0.41±0.55	-0.38±0.43***	-0.39±0.38	-0.40±0.44	-0.40±0.40	-0.40±0.41	-0.41±0.51
Ramp Firing Frequency (Hz)	7.27±0.34***	6.09±0.27	4.51±0.19	9.31±0.42***	8.06±0.26	6.80±0.25	9.02±0.33***	7.42±0.26	5.59±0.18
Phasic Spiking (proportion)	0.45±0.01***	0.51±0.01	0.60±0.02	0.36±0.01***	0.43±0.01	0.48±0.01	0.36±0.01***	0.45±0.01	0.56±0.01

Figure S5. Functional analysis using Optopatch: Additional analysis. Related to Figure 1D. *KCNQ2-01-het par* and "corrected" clones *-G6* and *-A6* iPSCs were differentiated into cortical excitatory neurons and transduced with CheRiff and QuasAr3 for Optopatch experiments. (A) Neurons were stimulated with blue light with increasing intensity steps (0, 2.44, 5.5, 14.67, 33, and 88 mW/cm^2) and the firing frequency was recorded optically. The well wide firing frequency of neurons (~85 neurons per well, ~4000 neurons total) under a blue-light illumination protocol was analyzed across two independent experiments shown here and one additional biological replicate (shown in Figure 1D). *KCNQ2-01-G6* neurons exhibited a significantly lower firing frequency relative to *KCNQ2-01-het* parental patient-derived neurons, whereas *KCNQ2-01-A6* neurons exhibited higher firing frequency relative to *KCNQ2-01-het* parental patient-derived neurons across the stimulation protocols and independent differentiations. (B) Table of other Optopatch metrics analyzed show additional divergent parameters across three independent experiments for the two isogenic "corrected" clones. A t-test or Mann-Whitney test was used to make comparisons between *KCNQ2-01-A6 and KCNQ2-01-G6* (*p < 0.05, **p < 0.005 and ***p < 0.0005). All data are reported as means ± SEM (n = 48 wells analyzed per cell line, N = 1 independent experiment, cohort 2 on left and cohort 3 on the right).

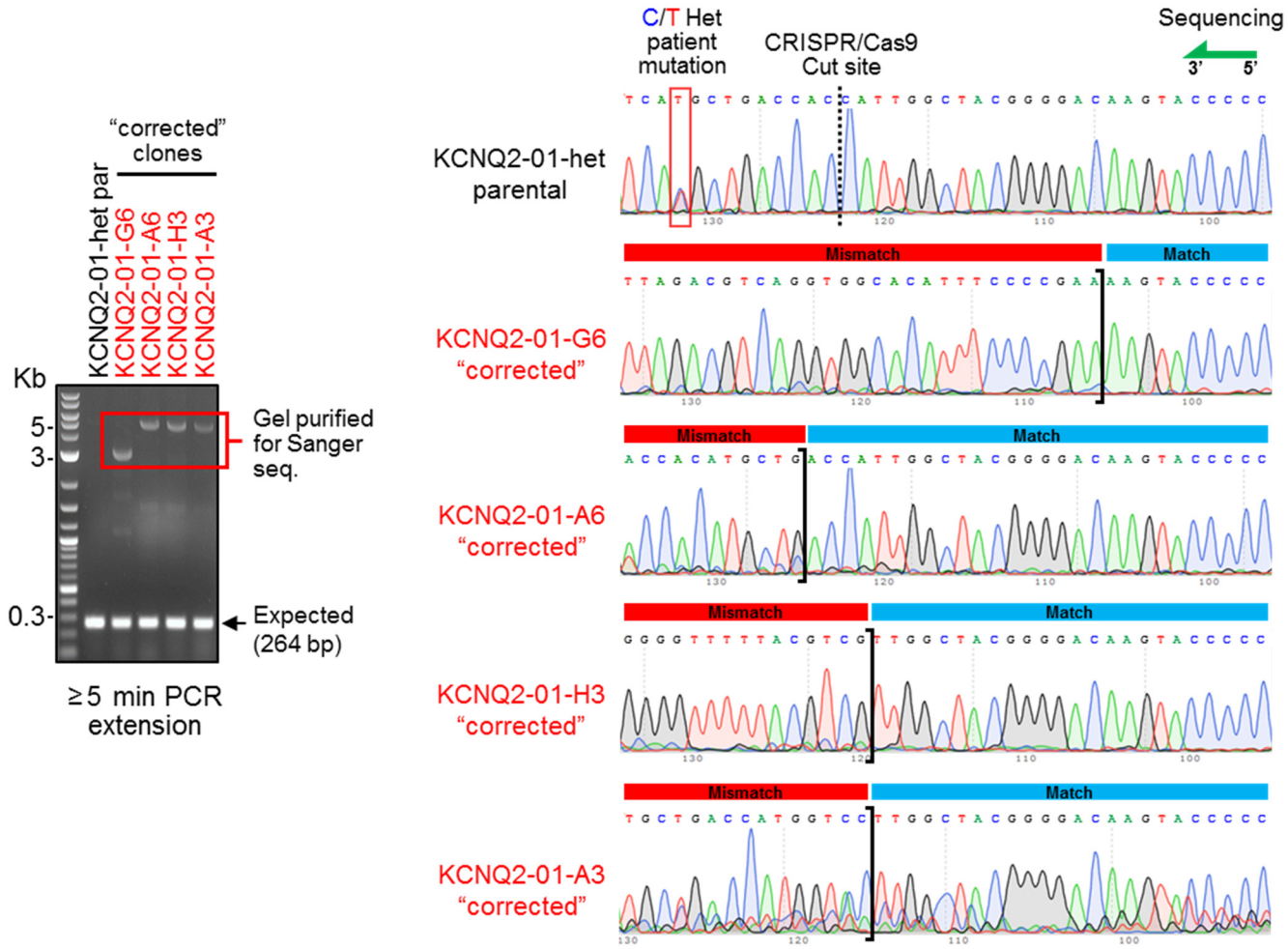

Figure S6. PCR and Sanger sequencing of target loci and deleterious insertions. Related to Figure 1F. Long extension PCR of 264 bp fragment and gel extraction and purification of upper band in the gel (left). Sanger sequencing of insertions revealed different sequences inserted near the cut site in clones *KCNQ2-01-G6*, *-A6*, *-H3* and *-A3*. Sequencing revealed initial sequence that matched the parental line (indicated with a blue bar above each chromatogram). Black bars indicate the beginning of mismatched sequence for each edited clone.

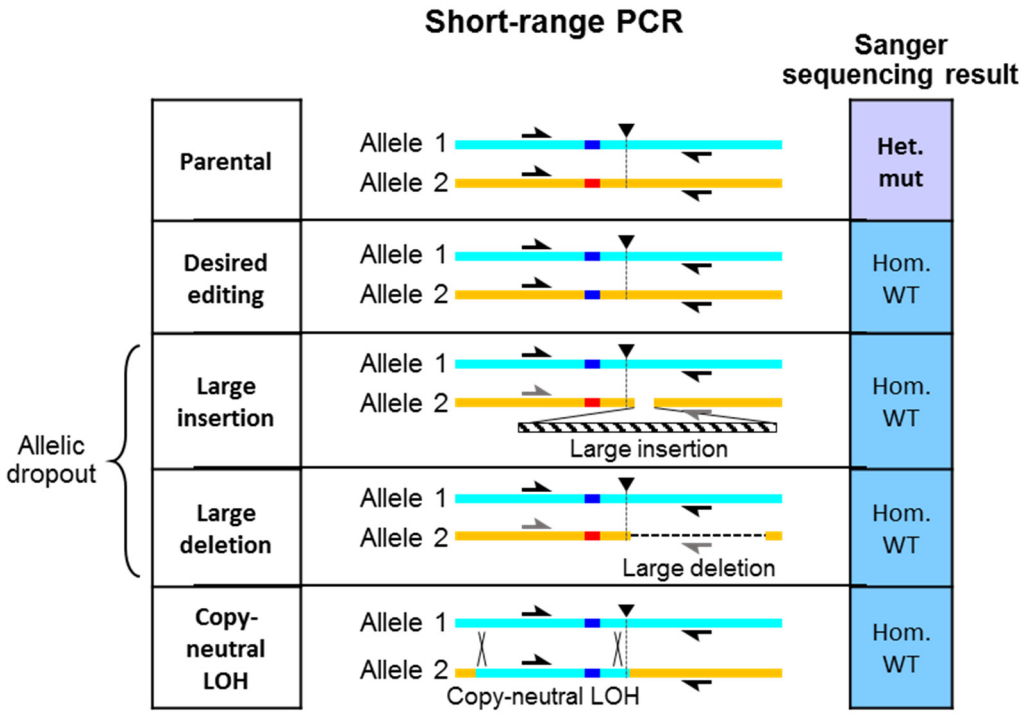

Figure S7. Illustration of Sanger sequencing results with different scenarios using standard short-range PCRs. Related to Figure 1, 2 and 4. Short-range PCR does not allow for distinction of true homozygous clone vs. mono-allelic PCR amplification (allelic dropout) due to large structural variants.

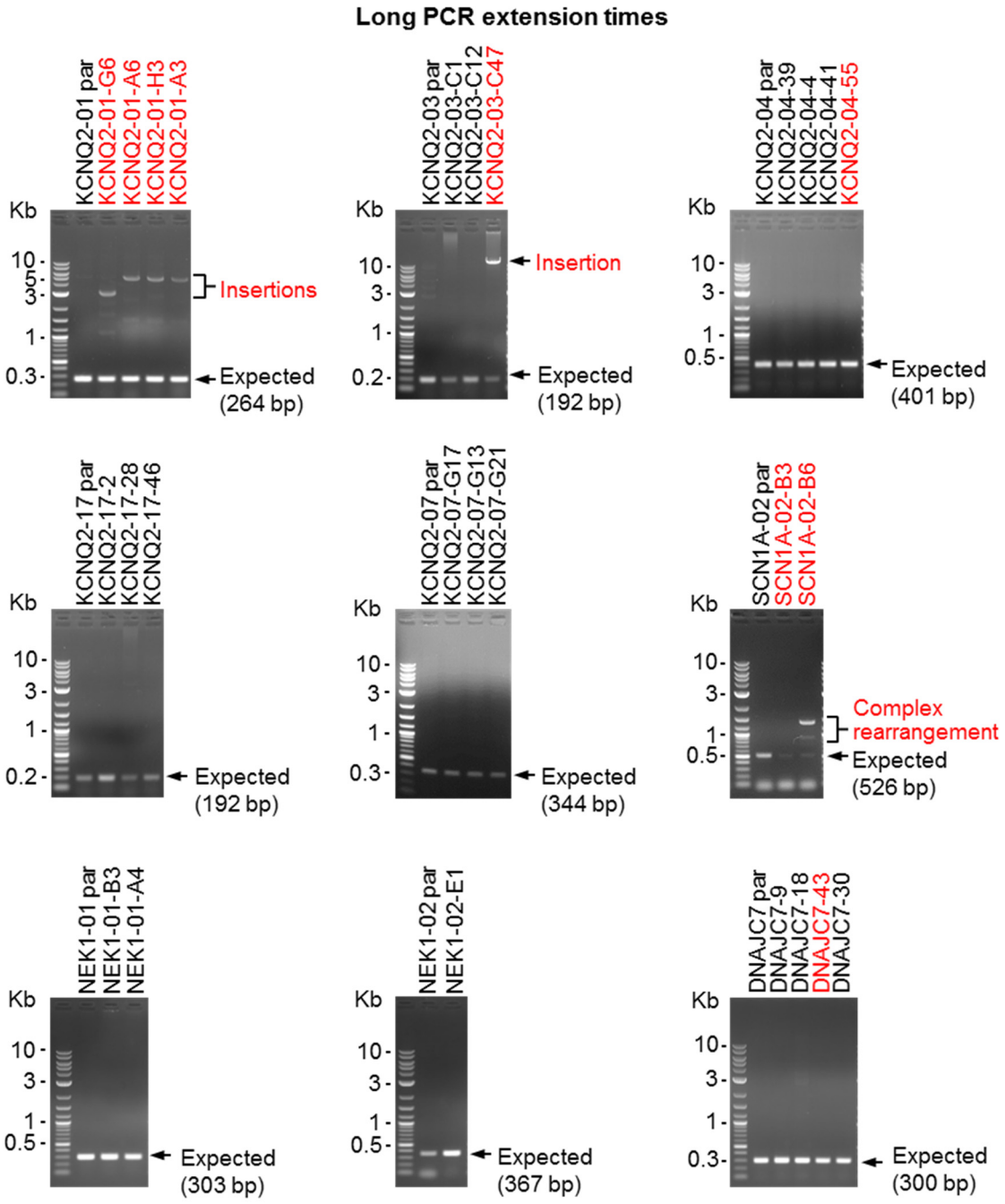

Figure S8. Detection of insertions by increased PCR extension times. Related to Figure 1. PCR fragments generated by amplifying expected 200-500 bp spanning the target loci with increased PCR extension times were run on agarose gels. Edited clones generated from 9 targeting events were compared to their respective parental untargeted lines. This method allowed for the detection of 6 clones with on-target insertions.

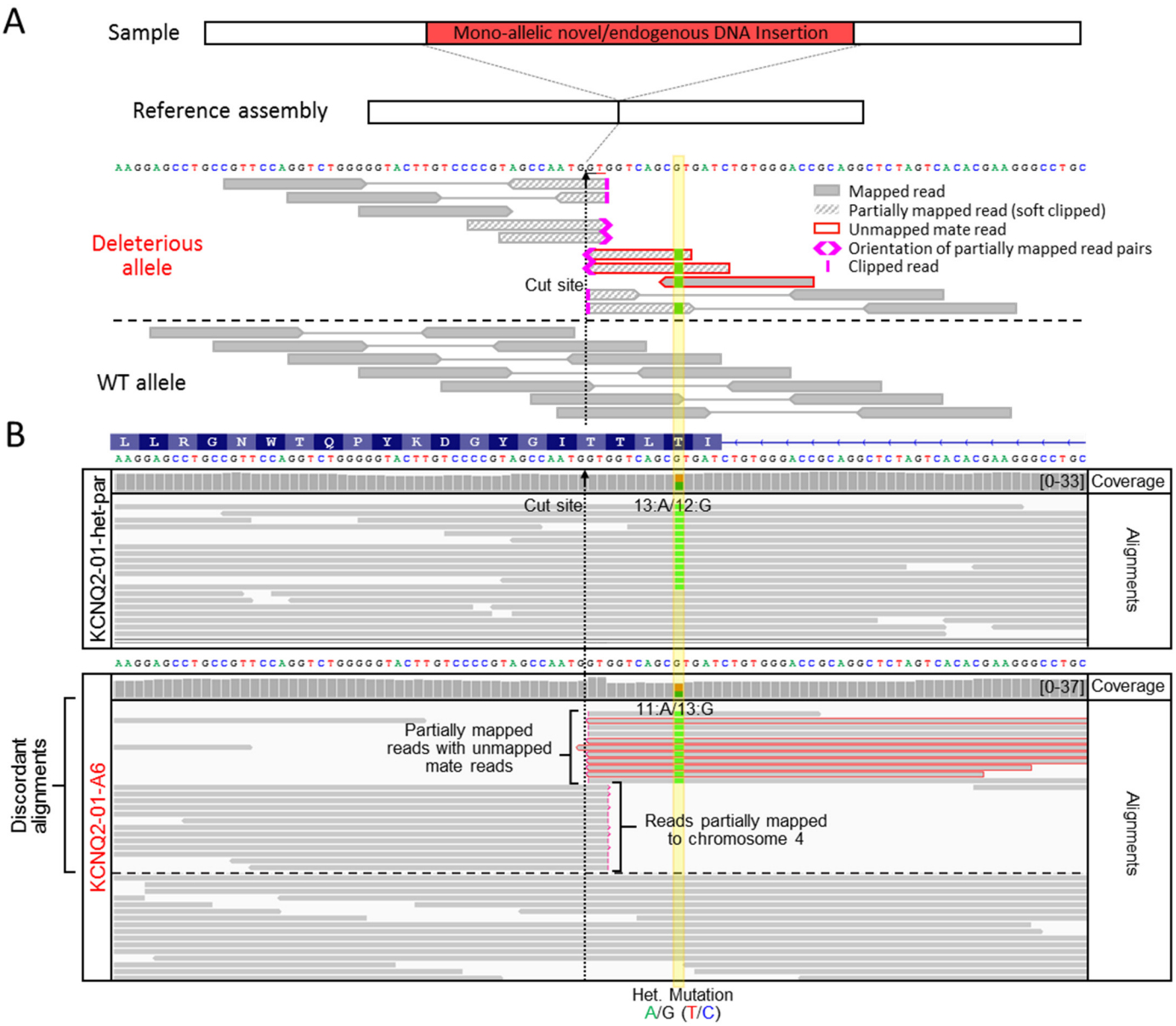

Figure S9. Whole genome sequencing (WGS) can help identify specific deleterious on-target effects of CRISPR/Cas9 editing and detect clones falsely identified as "corrected". Related to Figure 3. (A) Illustration of paired-end WGS alignments in the presence of a mono-allelic structural variant such as the large on-target insertion in *KCNQ2-01-A6*. (B) WGS Integrative Genomic Viewer (IGV) plot showing human genome (T2T) reference assembly mapped sequencing reads around the targeted locus of *KCNQ2-01-het-parental* and *-A6* edited line. WGS analysis revealed the presence of the heterozygous patient mutation in both *KCNQ2-01-G6* and *KCNQ2-01-A6* clones (see Figure 3) that had appeared to be "corrected" by Sanger sequencing in Figure 1B. When alignments are grouped by concordance to reference assembly, partially mapped reads are displayed at the top. Reads with unmapped mates are outlined in red. Sequence alignment stops abruptly at the Cas9 cut site, with soft clipped bases from both sides. On one side of the Cas9 cut site are reads with unmapped mates with sequences that are homologous to Cas9 carrying plasmid used to target this locus. From the other side of the cut site are reads with soft clipped bases and mates that align to a region of chromosome 4. This suggests the presence of both unmapped plasmid DNA and human chromosome 4 DNA inserted at the target locus.

SUPPLEMENTAL TABLES

Table S1. Single guide RNA (sgRNA) and single stranded oligo donor (ssODN) sequences. Related to Figure 1.

Target Locus	sgRNA (Sequence 5'-3' and NGG, red = bases targeted for editing)	ssODN (Sequence 5'-3', blue = intended mutation, red = intended CRISPR/Cas9-blocking mutation)
KCNQ2-01	CAGATCATGCTGACCACCAT TGG	AGTCGCCAGCGGGCGTCCAGCCTGCCCTCAGGGGTGTGAGCAGGCCCTTCGTG TGACTAGAGCCTGCGGTCCCACAGATCAcGCTGACCACtATTGGCTACGGGGACA AGTACCCCCAGACCTGGAACGGCAGGCTCCTTGCGGCAACCTTCACCCTCATCG G
KCNQ2-03	GATTCTGAGGATGATCCGCA TGG	GCTGGCCGCCGGCTCCCAGGGCAACGTCTTTGCCACATCTGCGCTCCGGAGCCT GCGCTTCCTGCAGATTCTGcGGATGATCCGaATGGACCGGCGGGGAGGCACCTG GAAGCTGCTGGGCTCTGTGGTCTATGCCCACAGCAAG
KCNQ2-04	TAATTTGGGACAGCATGTCC AGG	AGTGGGCTTTGTCCCAGAAGCCCACCCCGTTCTTGTCCCCTGCTGGACAGGCAG GCGGGGCTCTTGCCTGGACTGCAGGCTCTTAATTcGGGACAGCATGTCCAGaTGG CCaGCTGAGTACTGCTCGATGACGTCCATCACGTCGTAGGGCCGCAGGCTCTCCT TGAACTTCCGCTTGGACACCAGGAAC
KCNQ2-07	GGGGGACACCTGGACTCACC TGG	GAAGGTTCAGGAGCAGCACAGGCAGAAGCACTTTGAGAAGAGGCGGAACCcGGC AGCAGGCCTGATaCAGGTGAGTCCAGGTGTCCCCCGGGGACCAGCACAGCCCTT GTCCTGGTCCCACCTTGTTGAGGAG
KCNQ2-17	GGCCGTGACTCACCTTGCTG CGG	ATGGACCGGCGGGGAGGCACCTGGAAGCTGCTGGGCTCTGTGGTCTATGCgCaC AGCAAGGTGAGTCACGGCCCCAAGGCTGGCGGTGGGCGCCCCC
SCN1A-02	AAAGATCATCGGCAATTCCG TGG	CAAAATCTTGGCCAACGTTAAATATGCTAATAAAGATCATCGGCAATTCCGTcGGG GCTCTGGgAAATTTAACCCTCGTCTTGGCCATCATCGTCTTCATTTTTGCCGTGGT CGGCATGCAGCTCTTTGGTAAAAGCTACAAAGATTGTGTCTGCAAGATCGCC
NEK1-01	TGAAAAGTTTCTCTCTCCTC AGG	GCAGTTTGGTGTCTCAGTTATTTAAAAGAAATCCTAGGGATAGACCATCAGTCAAC TCCATATTGGAGAAAGGTTTTATAGCCAAACgCATTGAAAAGTTTCTCTCTCCTCAa GTAAGTTCTTTTTCCTTTAAAATTAAACAGTAGGGTTATGTTGCTTAGCTAAGACAT GGCCTCCAGTGTTGAGGAGAAC
NEK1-02	TAGCTTCCCGTTTTCGCTGC AGG	CAAACAAAATTCATACCATATGTCCTTCGGCTCGAGCTTTATTCTGCATAGCTTCC CGTTTTCaCTGCAGGAACTCTTCTACTTGTTTAGCTCTTTCTAC
DNAJC7-01	g1:TGAGAAGCGAGATTTTCGGA AGG	ssODN1mut:ATTTTGCGACAAAGAGCAGATGAGATTATCTCATGGTTGTACTGTACC TTtCGgAAATCTCaCTTCTCAAAATCTGTTTCTGCTATTTTCTCATATTCCATGACTG CATTAG
	g2:ATTTTGAGAAGCGAGATTTT CGG	ssODN2wt:ATTTTGCGACAAAGAGCAGATGAGATTATCTCATGGTTGTACTGTACCT TtCGgAAATCTCgCTTCTCAAAATCTGTTTCTGCTATTTTCTCATATTCCATGACTGC ATTAG

Table S2. Primer sequences for PCR amplification. Related to Figure 1 and 2.

Target Locus	Primers for short-range PCR (Sequence 5'-3') *Used for gels in Figure S8		Primers for Long-range PCR (Sequence 5'-3')	
KCNQ2-01	Forward:	GCCTACAAGACCTCGTCCC	Forward:	CAGTGGTCACTGCACGCTAC
	Reverse:	CGCATCTGTCCCATCCCAA	Reverse:	TTCCTGATTCAAACGCGCTG
	Size:	264 bp	Size:	4495 bp
KCNQ2-03	Forward:	CACCTTGCTGTGGGCATAGA	Forward:	CCATAAGGCTTAGTAACTCTCTGA
	Reverse:	GCCCGCTTTGTAGACATCA	Reverse:	ATCAAGGAGTATGAGAAGAGCTC
	Size:	192 bp	Size:	5346 bp
KCNQ2-04	Forward:	CAGACAAGAGGGGCAAGTCC	Forward:	GACAATAAGAAGGGAGGGAGGC
	Reverse:	AACAGAAGCTGACAGAGGCC	Reverse:	TCCATTGGCCAGAATGTCCTTT
	Size:	401 bp	Size:	5063 bp
KCNQ2-07	Forward:	CAGGGGTTGGAGCCATTTCT	Forward:	CTGGATTTCCGTTCTCTATGCCT
	Reverse:	CCCTGATGAATTGGGGTGTGG	Reverse:	TGGCTCCTTCTGGAAGTTTCTTT
	Size:	344 bp	Size:	11574 bp
KCNQ2-17	Forward:	CACCTTGCTGTGGGCATAGA	Forward:	CCATAAGGCTTAGTAACTCTCTGA
	Reverse:	GCCCGCTTTGTAGACATCA	Reverse:	ATCAAGGAGTATGAGAAGAGCTC
	Size:	192 bp	Size:	5346 bp
SCN1A-02	Forward:	AAATTAGCCATGAGCCTGAGAC	Forward:	TACTAAGGATGAGAAAACTCACACG
	Reverse:	AAAATGCATATCTTAAGTGGGTACAT	Reverse:	GCATCATGCATAACAACCTGCAT
	Size:	526 bp	Size:	5162 bp
NEK1-01	Forward:	ACCATTCCTCCAAGATCCAGATG	Forward:	TGTGAATTGAGAGATGGGGCAT
	Reverse:	TTGAAGCTGGCAGTATGAAAAACC	Reverse:	CAAACTAGACATCTGGCTCCCA
	Size:	303 bp	Size:	5508 bp
NEK1-02	Forward:	GACTTCTGAGTATCTTTACTGCCTC	Forward:	AGTGGGGGACATGGAAGGTA
	Reverse:	CAGAGATAGTGTTTCATCAGCCTTC	Reverse:	TGGATGTGAGGCATGCAGTT
	Size:	367 bp	Size:	6023 bp
DNAJC7-01	Forward:	TATTCTAGAGCTTTTGTGCCATACT	Forward:	ATCATGGGGATCGTCAGTGC
	Reverse:	AAGAGGCAGTGTGGTATATTTACTG	Reverse:	GGCTGGGTTGCTACAGTTGA
	Size:	300 bp	Size:	4430 bp

Table S3. Predicted off-target sequences for KCNQ2-01 single guide RNA and PCR primers for T7 assay or sequencing. Related to Figure S4.

Predicted off-target sequence (CAGATCATGCTGACCACCATTGG)	Mis matches	UCSC gene	Locus	Gene		PCR primer set	Size (bp)
CAGATCACGCTGACCACCATTGG	1MMs [8]	NM_172107	chr20:-62071037	KCNQ2	F	AACTAAGCACAACCCCTGGG	1150
					R	TCTGCAGGCCCATCTTGAAG	
CAGATCATGATGACCACCAGCAG	2MMs [10:20]	NM_020822	chr9:-138651650	KCNT1	F	GCACACATATATTCACAAACATGGC	842
					R	GGACAAGAGAAGGGAACTCACA	
CAGATCACACTGGCCACCATTGG	3MMs [8:9:13]	NM_004519	chr8:-133186572	KCNQ3	F	CCTGGCTGTGGATGGGAAAT	867
					R	ATCCCCTGCTCCCAGAGAAT	
CACACCATGCTGACGACCATGAG	3MMs [3:5:15]	NM_015868	chr19:-55250012	KIR2DL3	F	GACGTCTTTTGAGTCTGGTCG	328
					R	ATCTCCATCCCCGCACT	
CTGATCATGAAGACCACCAGGGG	4MMs [2:10:11:20]	NM_017994	chr7:-66406902	TMEM248	F	CTGTTGGCAAGTCAGTCCTTG	297
					R	TATATGGCAAGCCACAGGGTG	
CAGAACATGCTGACCACAAAGGG	3MMs [5:18:20]	NM_015016	chr19:-18241435	MAST3	F	CAGCGCTTTGCCATCAAGAAG	270
					R	ACAGAACAGACCTCAACTTGGT	
CAGACCATCCTGAGCACCATAGG	3MMs [5:9:14]	NM_003589	chr13:+113265345	CULV4A	F	CCAGGTAGTGACAAGTGGGTC	632
					R	GCATTTCTGTCTAAGTGCTGTTTC	
CTACTCATGTTGACCACCATTGG	4MMs [2:3:4:10]	NM_014038	chr7:+166577264	BZW2 intronic	F	TGCTCGTGACTCTTTGAGAATTG	276
					R	GACTTTGAGAAAACAATGACATGC	
CAGATCATGCTGGGCACCATAGG	2MMs [13:14]	NM_181678	chr5:-146055894	PPP2R2B intronic	F	CCAGGTAGTGACAAGTGGGTC	297
					R	GCATTTCTGTCTAAGTGCTGTTTC	
AAGGTCATCCTGACCACCATAAG	3MMs [1:4:9]	NA	chr11:-44370967	intergenic	F	AGCTCTGGAAAGCTGCCTTATC	204
					R	GAGACAGTCCAAGACGTGGC	
CACATCCTGGTGACCACCATCAG	3MMs [3:7:10]	NA	chr11:-115764718	intergenic	F	GGTCTTGGCATGCCTTTCTG	207
					R	TCTGTCTTCCAACCCTGGCT	
CAGTACATGCTGACCACCCTTAG	3MMs [4:5:19]	NA	chr2:-26065149	intergenic	F	GAACACAGAACACTACAACAAACT	277
					R	AGGTAGTAAAGTGTGAATCATCAGA	

Table S4. Primer and probe sequences for qgPCR allele copy number assay. Related to Figure 2.

	Assay set 1 (Sequence 5'-3')				Assay set 2 (Sequence 5'-3')			
Target Locus		**Primer/Probe sequences**	**Distance from target (bp)**	**Amplicon Size**		**Primer/Probe sequences**	**Distance from target (bp)**	**Amplicon Size**
KCNQ2-01	Forward	GGGAAGAGGAGAGAGGGCTCAG	179	370	Forward	CTCACTGGGCCTCCGTGTGGAT	126	353
	Reverse	GTCACCTCGGGAGCCTACAAGA	148		Reverse	AGGTCCCACCTAGGGAACTGTGC	183	
	6-FAM/ZEN/IBFQ Probe	TCACCCTCATCGGTGTCTCCTTCT	69		6-FAM/ZEN/IBFQ Probe	TCACCCTCATCGGTGTCTCCTTCT	69	
KCNQ2-03	Forward	CTCTGCACATCCTCCTGGAA	181	375	Forward	GCCCGCTTTGTAGACATCAT	98	351
	Reverse	CCAGGGCTCTTGAAGCAAAC	155		Reverse	GAGGCTCGTTCACACCTGAT	214	
	6-FAM/ZEN/IBFQ Probe	CCACGCCCGCTTTGTAGACATCAT	91		6-FAM/ZEN/IBFQ Probe	AACGTCTTTGCCACATCTGCGC	30	
KCNQ2-04	Forward	TCTCAGAGGTGCTAGGAAGG	174	364	Forward	AGGTCTCAGAGGTGCTAGGAAG	175	369
	Reverse	ACACAACAGAAGCTGACAGAG	150		Reverse	AGACACAACAGAAGCTGACAGAG	150	
	6-FAM/ZEN/IBFQ Probe	TGTCCAAGCGGAAGTTCAAGGAGA	70		6-FAM/ZEN/IBFQ Probe	TCCAAGCGGAAGTTCAAGGAGAGC	68	
KCNQ2-07	Forward	GGTCTGACCCTGATGAACTG	259	366	Forward	GGTGTGTGAGTCTCTGGAGT	191	364
	Reverse	CTCCACTCCTCAACAAGGTG	68		Reverse	AGATTCCTGCAGAGGGTGAG	134	
	6-FAM/ZEN/IBFQ Probe	TGACCTGACCCTGATGAATTGCAGG	76		6-FAM/ZEN/IBFQ Probe	TTGTCCTGGTCCCACCTTGTTGAG	56	
KCNQ2-17	Forward	CTCTGCACATCCTCCTGGAA	245	375	Forward	GCCCGCTTTGTAGACATCAT	162	351
	Reverse	CCAGGGCTCTTGAAGCAAAC	91		Reverse	GAGGCTCGTTCACACCTGAT	150	
	6-FAM/ZEN/IBFQ Probe	CCACGCCCGCTTTGTAGACATCAT	162		6-FAM/ZEN/IBFQ Probe	AACGTCTTTGCCACATCTGCGC	94	
SCN1A-02	Forward	CTTGGCCAACGTTAAATATGCTAAT	33	382	Forward	GACCATTTCTAGGTAAAGCTCAAT	137	384
	Reverse	TGTGCCATGCTGGTGTATTT	305		Reverse	TTGACCAGCAACCTCCATAC	204	
	6-FAM/ZEN/IBFQ Probe	TGTGTCTGCAAGATCGCCAGTGAT	83		6-FAM/ZEN/IBFQ Probe	TGTGTCTGCAAGATCGCCAGTGAT	83	
NEK1-01	Forward	ATTTAGTTTGAAGCTGGCAGTATG	158	362	Forward	TTGGAAGAGGATTGTGTTTCTATTC	270	388
	Reverse	AAAGAAAGACCATGGAAAGGAAAG	157		Reverse	CACTGGAGGCCATGTCTTAG	74	
	6-FAM/ZEN/IBFQ Probe	TCCGCAGTTTGGTGTCTCAGTTAT	67		6-FAM/ZEN/IBFQ Probe	TCTCCGCAGTTTGGTGTCTCAGTT	69	
NEK1-02	Forward	GATAGTGTTTCATCAGCCTTCATATTC	150	361	Forward	GGATGGCTGACTTTGTGATTTG	66	392
	Reverse	CTTCTGAGTATCTTTACTGCCTCTT	160		Reverse	ACAGGTATGAACTTACTCCCAATTA	280	
	6-FAM/ZEN/IBFQ Probe	CAGGATGGCTGACTTTGTGATTTG	66		6-FAM/ZEN/IBFQ Probe	CCAAGTGAAGGTCTGGAATAAGGT	92	
DNAJC7-01	Forward	GCATTCGACCCTATCTCTATC	180	354	Forward	GAGCCCTAGAACTGGATCATAAA	226	358
	Reverse	AGTCAGAAGCCTAATTTAAGTG	132		Reverse	TTGTGCCATACTACTCCTCTTAAT	86	
	6-FAM/ZEN/IBFQ Probe	TTCCCATTCGTGTGTGTGTGTGAT	61		6-FAM/ZEN/IBFQ Probe	TATCACACACACACACGAATGGGA	62	

Table S5. Overview of CRISPR/Cas9-edited iPSC clones and QC analysis findings. Related to Figures 1, 2 and 3. Clones with on-target defects are denoted in red.

Gene	Locus	Cell Line abbreviations	Short-range PCR w/ long extension times	Long-range PCR & het. SNP Sanger sequencing	qgPCR allele copy #	WGS analysis
KCNQ2	1	**KCNQ2-01-het parental**		Het. SNPs present	2	Analyzed; unedited clone
		KCNQ2-01-G6	~3 kb on-target insertion	LOH	1	Analyzed; 17 bp deletion and large plasmid DNA insertion
		KCNQ2-01-A6	~5 kb on-target insertion	LOH	1	Analyzed; Large plasmid and endogenous (human chromosome 4) DNA insertion
		KCNQ2-01-H3	~5 kb on-target insertion	LOH	1	Not analyzed
		KCNQ2-01-A3	~5 kb on-target insertion	LOH	1	Not analyzed
	2	**KCNQ2-03-het parental**		Het. SNPs present	2	Analyzed; untargeted parental
		KCNQ2-03-het-C1		Het. SNPs present	2	Not analyzed
		KCNQ2-03-C47	~5 kb on-target insertion	LOH	1	Analyzed; 10 bp deletion and large mitochondrial DNA insertion
		KCNQ2-03-C12		Het. SNPs present	2	Analyzed; intended CRISPR/Cas9 editing
	3	**KCNQ2-04-het parental**		Het. SNPs present	2	Analyzed; untargeted parental
		KCNQ2-04-het-39		Het. SNPs present	2	Not analyzed
		KCNQ2-04-4		Het. SNPs present	2	Analyzed; intended CRISPR/Cas9 editing
		KCNQ2-04-41		Het. SNPs present	2	Not analyzed
		KCNQ2-04-55	Unable to detect	LOH	1	Analyzed; large mitochondrial DNA insertion
	4	**KCNQ2-17-het parental**		Het. SNPs present	2	Not analyzed
		KCNQ2-17-het-2		Het. SNPs present	2	Not analyzed
		KCNQ2-17-28		Het. SNPs present	2	Not analyzed
		KCNQ2-17-46		Het. SNPs present	2	Not analyzed
	5	**KCNQ2-07-het parental**		Het. SNPs present	2	Not analyzed
		KCNQ2-07-het-G17		Het. SNPs present	2	Not analyzed
		KCNQ2-07-G13		Het. SNPs present	2	Not analyzed
		KCNQ2-07-G21		Het. SNPs present	2	Not analyzed
SCN1A	1	**SCN1A-02-het parental**		Het. SNPs present	2	Not analyzed
		SCN1A-02-B3	Unable to detect	LOH	1	Not analyzed
		SCN1A-02-B6	Undetermined complex rearrangement	LOH	1	Not analyzed
NEK1	1	**NEK1-01-het parental**		Het. SNPs present	2	Not analyzed
		NEK1-01-B3		Het. SNPs present	2	Not analyzed
		NEK1-01-A4		Het. SNPs present	2	Not analyzed
	2	**NEK1-02-WT parental**		Het. SNPs present	2	Not analyzed
		NEK1-02-het-E1		Het. SNPs present	2	Not analyzed
DNAJC7	1	**DNAJC7-01-WT parental**		Het. SNPs present	2	Analyzed; untargeted parental
		DNAJC7-01-het-18		Het. SNPs present	2	Analyzed; intended CRISPR/Cas9 editing
		DNAJC7-01-het-30		Het. SNPs present	2	Analyzed; intended CRISPR/Cas9 editing
		DNAJC7-01-hom-43		Copy-neutral LOH affecting 1 nearby het. SNP	2	Analyzed; copy-neutral LOH: rs6503679 het. SNP (-68 bp from targeted base)
		DNAJC7-01-WT-9		Het. SNPs present	2	Not analyzed
		DNAJC7-01-WT-40		Het. SNPs present	2	Not analyzed

SUPPLEMENTAL EXPERIMENTAL PROCEDURES

Generation and maintenance of iPSCs

Patient iPSC lines were generated from peripheral blood mononuclear cells (PBMCs) isolated from whole blood following informed consent under protocols approved both by Ann & Robert H. Lurie Children's Hospital of Chicago and Northwestern University IRB (#2015-738). Reprogramming of PBMCs into iPSCs was performed at the Northwestern Stem Cell Core Facility using Invitrogen's CytoTune®-iPS 2.0 Sendai Reprogramming system (A16517, Thermofisher) as previously described (Simkin et al., 2021). Healthy control iPSC line CS20002 (DNAJC7-01-WT) was purchased from Cedar Sinai: https://biomanufacturing.cedars-sinai.org/product/cs0002ictr-nxx/. Healthy control line HPSI0114i-kolf_2 (NEK1-02-WT) was provided by https://www.hipsci.org/lines/#/lines/HPSI0114i-kolf_2. All iPSCs were grown on Matrigel with mTeSR1 media, maintained at 37°C and 5% CO2 and passaged weekly using Accutase (Sigma). All cell lines were regularly tested for presence of mycoplasma using MycoAlert PLUS Detection Kit (Lonza) and determined to be mycoplasma-free.

CRISPR/Cas9 genome editing of human iPSC lines

The NEK1-02-WT iPSC line was edited by Jackson Labs. All other human iPSC lines were edited by Applied StemCell Inc. (Milpitas, CA). Plasmid based editing: iPSCs were electroporated with a DNA mixture containing the plasmid expressing the respective single guide RNA (sgRNA) and Cas9 nuclease, a puromycin-expressing plasmid, and the single stranded oligo donor (ssODN). Cells were selected by puromycin for two days post transfection. RNP-based editing: one million patient iPSCs were electroporated with a mixture of sgRNA and Cas9 in the ribonucleoprotein format, and ssODN. All sgRNA and ssODN sequences can be found in Table S1. A small portion of the cell culture, presumably with mixed population, was subjected to PCR and Sanger sequencing analysis. Once the mixed culture showed repair with qualified HDR efficiency, the transfected cells were subjected to single cell cloning. After two weeks in culture individual colonies were picked and expanded. A fraction of cells from each clone was collected for genotyping analysis by PCR and Sanger sequencing. Positive clones were further expanded and submitted again for sequencing to confirm desired genotype. iPSC clones were then cryopreserved and shipped to our lab.

Genomic DNA PCR and Sanger sequencing

Initial PCR/Sanger sequencing screening of up to 100 single edited iPSC clones was performed by Applied StemCell Inc. Clones that passed this initial screen were sent to us for further assessment. We designed primers using Primer-BLAST online tool http://www.ncbi.nlm.nih.gov/tools/primer-blast and performed PCR on gDNA to amplify 200 to 4500 bp region around the CRISPR/Cas9 target site. PCR was performed using Phusion Hot Start II DNA Polymerase with 5X Phusion GC Buffer (ThermoFisher). We tested several primer annealing temperatures and used standard PCR extension durations of 15-30 sec per Kb depending on the expected size of PCR fragment. PCR extension times were increased to up to 6 minutes to detect potential insertions. PCR fragments were run on 1% agarose gels with 2-log DNA ladder (New England BioLabs Inc.) to confirm single bands. Sanger sequencing was done using the same primers used for amplification of gDNA and PCR fragments were sequenced in both directions. All primer sequences can be found in Table S2. All but one clone passed this QC assessment.

To identify heterozygous SNPs or indels near target locus, primers were designed to amplify a 4 to 11 Kb region spanning the targeted locus. Primers to then sequence every ~850 bases along the amplified PCR fragment were designed. The presences of heterozygous SNP or indel in parental line but not in edited lines indicates a loss of heterozygosity which may be due to large deletions or insertions preventing the amplification of desired region or copy-neutral LOH.

Genomic integrity and pluripotency assays

G-banding karyotype analysis and short tandem repeat (STR) profile analysis DNA fingerprinting assay was performed by Cell Line Genetics Inc; Karyostat™ analysis by ThermoFisher. We assessed iPSC pluripotency markers with immunocytochemistry as described previously (Simkin *et al.*, 2021).

Analysis of Off-Target Cas9 Sites

To assess potential off-target effects regions of homology to the sgRNA sequence were predicted through an online tool: CCTop CRISPR/Cas9 target online predictor https://cctop.cos.uni-heidelberg.de/ (Stemmer et al., 2015). We selected the top 10 potential off-target regions and amplified each one by targeted PCR of genomic DNA from edited and unedited clones, for further analysis either by Sanger Sequencing or by a T7 Endonuclease assay (Table S3). Each amplicon was purified using the Wizard® SV Gel and PCR Clean-Up System (Promega) and the concentration was determined using a Nanodrop 2000 Spectrophotometer (Thermo-Fisher). Amplicons (500 ng) from each potential off-target region were denatured by heating at 95ºC for five minutes and then allowed to cool to room temperature to allow for the amplicons to re-anneal. T7 endonuclease I (Genecopoeia) was then added to the re-annealed products and incubated for 60 minutes at 37ºC. The PCR products from the potential off-target sites and the positive control template were run on 2% agarose gel with 6x loading buffer and a 2-log DNA ladder (New England BioLabs Inc.). All off-target regions and primer sequences can be found in Table S3.

Quantitative genotyping PCR-based copy number assay

Primers were designed to amplify 350-400 bp around the targeted locus. The accompanying probes were carefully selected to be close but not overlap the target or any Cas9-blocking silent mutations. Design of the primers and probes was done using the IDT PrimerQuest tool. Two assay sets were designed for each targeted locus, prioritizing variety in primer and probe binding sites. Genomic DNA was freshly isolated from iPSCs using the DNeasy Blood & Tissue Kit (Qiagen, 69504) according to the manufacturer's protocol. 60 ng of genomic DNA was mixed with 2X PrimeTime Gene Expression Mastermix (IDT, 1055772), 20X human TERT TaqMan Copy Number Reference Assay (VIC reporter; ThermoFisher, 4403316) as internal reference and the designed PrimeTime qPCR primer/probe assay set (5′ reporter 6-FAM and Quencher ZEN and 3' Iowa Black FQ; 0.25 pmol/µl, HPLC-purified, IDT) was used per reaction. All qgPCR assays were performed in triplicate on the BioRad CFX Connect Real-Time PCR Detection System. Reactions were run for 2 minutes at 50°C, 10 minutes at 95°C, and 40 cycles of 15 seconds at 95°C and 1 minute at 60°C. Fluorescence was captured every cycle at 520 nm for FAM (probe) and at 554 nm for VIC (TERT internal control). Allele copy number was determined by normalizing cycle threshold (Ct) values to internal control (TERT reference) and ΔΔCt values calculated by normalizing edited clones to their corresponding unedited parental lines. All primer/probe sequences are listed in Table S4.

Whole Genome Sequencing

WGS was outsourced to Novogene Corporation Inc., as previously described (Simkin *et al.*, 2021). We performed sequencing analysis after aligning the reads to the complete telomere-to-telomere human reference genome T2T-CHM13 v.1,1 (Nurk et al., 2021). The T2T-CHM13 reference genome was obtained using long-read sequencing and provides > 200MB of new sequenced regions that were not previously possible to capture with short-read sequencing. It also improves coverage of complex regions and variation calling (Aganezov et al., 2021), delivering consensus sequences without the use of alternative contigs (i.e. sets of overlapping DNA segments that together represent a consensus region of DNA). This was important in our case because several of our targeted loci (on human chromosome 20 spanning the *KCNQ2* gene) were in regions for which alternative reference sequences existed in the hg38 reference assembly.

The alignment process was done using the Burrows-Wheeler Aligner (BWA; v.0.7.17) following the GATK best practices pipeline (DePristo et al., 2011), which was modified to make use of the new T2T-CHM13 reference genome. Briefly, variants from dbSNP in VCF format, used for modeling the base quality score recalibration (BQSR) step, were lifted over from hg38 to T2T-CHM13 using liftOver from the UCSC (Kent et al., 2002) and chain files provided by the T2T consortium (https://github.com/marbl/CHM13).

Integrative Genomic Viewer (IGV) was used to visualize alignment tracks and assess read coverage (Robinson et al., 2011). Reads with unmapped mates will be outlined in red when the “Flag unmapped pairs” option is selected in IGV (Figure 3 and S9). Insertions or translocated duplications with endogenous DNA, such as mitochondrial DNA or another chromosome, will not be flagged with red outlined reads since these reads can be mapped elsewhere within the reference genome. However, grouping reads by “reference concordance” or “chromosome of mate” option can still allow for visualizing deleterious genomic regions by identifying partially mapped reads or split reads with soft clipped ends and with secondary alignments in other reference assembly regions (Figures 4-5, S9).

Cortical Neuron Differentiation and Optopatch Measurements

iPSCs were differentiated into glutamatergic neurons using a previously described protocol based on *Ngn2* overexpression (Simkin *et al.*, 2021). Cryo-stocks of Ngn2 neurons (preserved on day 4) differentiated from KCNQ2-01-het patient and KCNQ2-01-G6 and -A6 iPSC lines were thawed and plated onto custom-made Poly-D-Lysine/Laminin pre-coated Ibidi cell culture plates (100,000 cells/cm^2) and co-cultured with primary C57BL/6 mouse cortical glial cells (30,000 cells/cm^2). These co-cultures were maintained in complete Neurobasal medium supplemented with 1x Gibco© N2, 1x Gibco© B27, 10ng/mL BDNF (R&D), 2µg/mL Doxycycline (Sigma) and 2% Hyclone^{TM} Fetal Bovine Serum. Primary glial cells were prepared as previously described (Di Giorgio et al., 2008). Cells were cultured for 30 days with complete medium exchanges every 3 days. Two weeks prior to all-optical electrophysiology (Optopatch) measurements, cells were transduced with lentiviral particles encoding Optopatch components CheRiff-BFP and QuasAr3-Citrine (Adam et al., 2019; Hochbaum et al., 2014), driven by the human *Synapsin I* promoter for neuronal-specific expression. Lentiviral preparation and transduction were carried out as previously reported (Werley et al., 2017a). Cells were recorded on day 35 with Optopatch imaging (Hochbaum *et al.*, 2014; Kiskinis et al., 2018; Werley *et al.*, 2017a) using a custom built, ultra-wide field fluorescence microscope described previously (Werley *et al.*, 2017a; Werley et al., 2017b). Cells were imaged in Tyrodes Buffer (10mM HEPES, 125mM NaCl, 2mM KCl, 3mM $CaCl_2$, 1mM $MgSO_4$, 30mM Glucose, pH 7.4) in the presence of synaptic

blockers (10μM NBQX (Sigma), 25μM D-AP5 (Tocris) and 20μM Gabazine (Sigma) to block AMPA, NMDA and GABA currents, respectively) to allow for measurements of intrinsic spontaneous and evoked neuronal activity. Briefly, samples were illuminated with ~100 W/cm^2 635 nm laser excitation to monitor changes in membrane potential through changes in QuasAr3 fluorescence. In order to evoke neuronal activity, a custom blue light (470nm LED) stimulus protocol was used to depolarize the cell membrane through excitation of CheRiff. The stimulus protocol consisted of 2 seconds of spontaneous activity (blue light off) followed by five 500 msec steps of increasing blue light intensity (2.45, 5.5, 14.67, 33, and 88 mW/cm^2), with 500 msec of rest in between each stimulus step. Imaging data were recorded on a Hamamatsu ORCA-Flash 4.0 sCMOS camera across a 4 mm x 0.5 mm field of view at a 1 kHz frame rate. Data acquisition was performed using custom control software written in MATLAB. Analysis of Optopatch data, using a custom analytics pipeline written primarily in MATLAB, was carried out as previously described (Werley *et al.*, 2017a). Statistical significance/p-values were determined using t-tests or Mann-Whitney tests where appropriate with a custom MATLAB routine (*p < 0.05, **p < 0.005 and ***p < 0.0005, respectively). All data are reported as means ± SEM.

SUPPLEMENTAL REFERENCES

Adam, Y., Kim, J.J., Lou, S., Zhao, Y., Xie, M.E., Brinks, D., Wu, H., Mostajo-Radji, M.A., Kheifets, S., Parot, V., et al. (2019). Voltage imaging and optogenetics reveal behaviour-dependent changes in hippocampal dynamics. Nature *569*, 413-417. 10.1038/s41586-019-1166-7.

Aganezov, S., Yan, S.M., Soto, D.C., Kirsche, M., Zarate, S., Avdeyev, P., Taylor, D.J., Shafin, K., Shumate, A., Xiao, C., et al. (2021). A complete reference genome improves analysis of human genetic variation. bioRxiv, 2021.2007.2012.452063. 10.1101/2021.07.12.452063.

DePristo, M.A., Banks, E., Poplin, R., Garimella, K.V., Maguire, J.R., Hartl, C., Philippakis, A.A., del Angel, G., Rivas, M.A., Hanna, M., et al. (2011). A framework for variation discovery and genotyping using next-generation DNA sequencing data. Nature genetics *43*, 491-498. 10.1038/ng.806.

Di Giorgio, F.P., Boulting, G.L., Bobrowicz, S., and Eggan, K.C. (2008). Human embryonic stem cell-derived motor neurons are sensitive to the toxic effect of glial cells carrying an ALS-causing mutation. Cell Stem Cell *3*, 637-648. 10.1016/j.stem.2008.09.017.

Hochbaum, D.R., Zhao, Y., Farhi, S.L., Klapoetke, N., Werley, C.A., Kapoor, V., Zou, P., Kralj, J.M., Maclaurin, D., Smedemark-Margulies, N., et al. (2014). All-optical electrophysiology in mammalian neurons using engineered microbial rhodopsins. Nature methods *11*, 825-833. 10.1038/nmeth.3000.

Kent, W.J., Sugnet, C.W., Furey, T.S., Roskin, K.M., Pringle, T.H., Zahler, A.M., and Haussler, D. (2002). The human genome browser at UCSC. Genome Res *12*, 996-1006. 10.1101/gr.229102.

Kiskinis, E., Kralj, J.M., Zou, P., Weinstein, E.N., Zhang, H., Tsioras, K., Wiskow, O., Ortega, J.A., Eggan, K., and Cohen, A.E. (2018). All-Optical Electrophysiology for High-Throughput Functional Characterization of a Human iPSC-Derived Motor Neuron Model of ALS. Stem Cell Reports *10*, 1991-2004. 10.1016/j.stemcr.2018.04.020.

Nurk, S., Koren, S., Rhie, A., Rautiainen, M., Bzikadze, A.V., Mikheenko, A., Vollger, M.R., Altemose, N., Uralsky, L., Gershman, A., et al. (2021). The complete sequence of a human genome. bioRxiv, 2021.2005.2026.445798. 10.1101/2021.05.26.445798.

Robinson, J.T., Thorvaldsdottir, H., Winckler, W., Guttman, M., Lander, E.S., Getz, G., and Mesirov, J.P. (2011). Integrative genomics viewer. Nat Biotechnol *29*, 24-26. 10.1038/nbt.1754.

Simkin, D., Marshall, K.A., Vanoye, C.G., Desai, R.R., Bustos, B.I., Piyevsky, B.N., Ortega, J.A., Forrest, M., Robertson, G.L., Penzes, P., et al. (2021). Dyshomeostatic modulation of Ca(2+)-activated K(+) channels in a human neuronal model of KCNQ2 encephalopathy. Elife *10*, e64434. 10.7554/eLife.64434.

Stemmer, M., Thumberger, T., Del Sol Keyer, M., Wittbrodt, J., and Mateo, J.L. (2015). CCTop: An Intuitive, Flexible and Reliable CRISPR/Cas9 Target Prediction Tool. PLoS ONE *10*, e0124633. 10.1371/journal.pone.0124633.

Werley, C.A., Brookings, T., Upadhyay, H., Williams, L.A., McManus, O.B., and Dempsey, G.T. (2017a). All-Optical Electrophysiology for Disease Modeling and Pharmacological Characterization of Neurons. Curr Protoc Pharmacol *78*, 11 20 11-11 20 24. 10.1002/cpph.25.

Werley, C.A., Chien, M.P., and Cohen, A.E. (2017b). Ultrawidefield microscope for high-speed fluorescence imaging and targeted optogenetic stimulation. Biomed Opt Express *8*, 5794-5813. 10.1364/BOE.8.005794.